Article

Improved Instantaneous Current Value-Based Protection Methods for Faulty Synchronizations of Synchronous Generators

Kumar Mahtani [1,*], José M. Guerrero [2] and Carlos A. Platero [1]

1   Department of Electrical Engineering, Escuela Técnica Superior de Ingenieros Industriales, Universidad Politécnica de Madrid, 28006 Madrid, Spain; carlosantonio.platero@upm.es
2   Department of Electrical Engineering, Escuela de Ingeniería de Bilbao, Universidad del País Vasco, 48013 Bilbao, Spain; josemanuel.guerrerog@ehu.eus
*   Correspondence: kumar.mahtani@upm.es

Abstract: Faulty synchronizations of synchronous generators can cause significant detrimental effects, primarily due to a large current and high electromagnetic torque. These effects not only impact the generator but they can also extend to the prime mover and the step-up transformer. Furthermore, such events can trigger disturbances in the power system, potentially leading to system collapse if not promptly cleared. Although the autosynchronizers and synchro-check technologies are well established in the industry, faulty synchronizations, such as those caused by incorrect wiring during maintenance or commissioning operations, can go undetected by these systems. Existing protections do not allow for the detection of faulty synchronizations in a timely manner. This paper presents novel protection methods specifically designed for this issue: one based on instantaneous current value and the other on the instantaneous current-derivative value. These schemes are activated exclusively during the synchronizations process, allowing for faster fault detection compared to existing methods, thereby reducing the duration of harmful electrical and mechanical stresses after a faulty synchronization. The effectiveness of the proposed schemes has been validated through computer simulations of a 362 MVA turbo-generator from a thermal power plant and also through experimental tests on a 5 kVA synchronous generator using a specialized laboratory synchronization test bench, yielding promising results.

Keywords: power generation; power system protection; power system transients; synchronization; synchronous generator

1. Introduction

The process of connecting synchronous generators (SGs) to a running power system, known as grid synchronization [1,2], illustrated in Figure 1, must be conducted in a way to minimize detrimental electrical and mechanical stresses on the SG and maintain stability within the power system. To achieve this, it is essential to ensure that the voltage magnitude, voltage phase angle, frequency, and phase-sequence are aligned at the moment when the generator circuit breaker, CB (ANSI 52G), is closed.
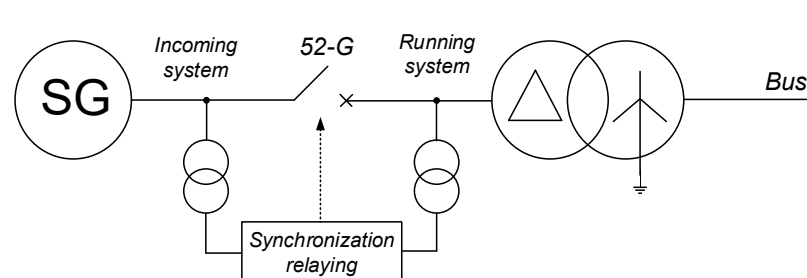
Figure 1. Simplified one-line diagram of SG synchronization.

Deviations in the mentioned parameters during synchronization, referred to as faulty synchronizations, can lead to high currents, resulting in excessive heating and mechanical forces that can potentially damage SG winding insulation, the stator bracing and bolts, and even the coupling between the SG and the turbine given the high torsional effect [3–7]. Additionally, the stresses imposed on the grid in these events can cause oscillations and voltage instability [8,9], leading to broader system reliability issues. In fact, catastrophic events have been reported in the literature due to faulty synchronizations [10–12].

Modern synchronizing systems [13,14] offer both manual and automatic control options via a selection switch (ANSI 43 M/A). In these systems, the governor and excitation control systems are interfaced with the contacts of the manual regulation switches and, in parallel, with those of the autosynchronizer (ANSI 25A). The autosynchronizer automates the synchronization process by continuously adjusting the SG's speed and voltage to bring them into synchronism with the grid. Furthermore, the synchronism-check relay (ANSI 25) supervises the process, whether performed under manual or automatic mode, by verifying that the differences in voltage magnitude, phase angle, and frequency are within acceptable limits at the synchronization instant. While synchronizers (ANSI 25A) aim to achieve precise synchronizations, synchronism checking (ANSI 25) helps to prevent faulty synchronizations. In this regard, the synchronism-check relay serves as a safeguard, preventing CB closing if the synchronization conditions are not met.

However, synchronism-check relays may not always detect faulty synchronizations. Particularly, the following cases can lead to out-of-phase synchronizations [3,15–17] that cannot be detectable by the checking schemes:

- Incorrect wiring in the main power circuit or in the voltage transformer (VT) circuits, which is the most common case;
- CB closing times longer than expected;
- Flash-over or arcing between the CB contacts due to reduced dielectric capacity (pollution, low pressure dielectric, humidity, insulator decomposition);
- The wrong setting on the synchronizing systems.

Therefore, synchronism-check relays are not sufficient to ensure successful synchronization, thus advanced protection mechanisms are needed to effectively detect faulty synchronizations. The proposed protection method, which is based on instantaneous synchronization current values, addresses this technical gap.

The main contributions of the present work are described hereunder.

1. This work identifies the critical gap in existing protections for the timely detection of faulty synchronizations, as current methods exhibit significant delays in fault detections.
2. The characteristics of the current and current derivative after a faulty synchronization are analyzed and described using a robust analytical framework.
3. Based on these characteristics, a novel protection scheme is proposed to address the identified gap, based on instantaneous current and current-derivative measurements. The method is validated through comprehensive computer simulations and experimental tests.
4. The proposed scheme requires only instantaneous current measurements and can be seamlessly commissioned by setting appropriate protection thresholds during system calibration.
5. The method achieves fault detection within 2–2.5 ms, significantly outperforming other root mean square (RMS)-based techniques that require several cycles for computation. This rapid response minimizes electrical and mechanical stresses during the most critical period following a faulty synchronization, offering enhanced protection for power generation assets and ensuring power system stability.

This paper is organized as follows. Section 2 analyzes faulty synchronizations and their effects. Section 3 describes the behavior of conventional protection functions during faulty synchronizations. Section 4 presents the operational principles of the proposed protection method. Section 5 describes the computer simulations, while Section 6 develops

the experimental tests. Finally, Section 7 concludes the paper by highlighting the main contributions and suggesting directions for future research.

2. Fundamentals of Faulty Synchronizations

2.1. Preliminary Aspects

The synchronization at $t = t_0$ of an SG delivering a sinusoidal electro-magnetomotive force at its terminals, V, is considered. The SG is considered to have speed $\omega_0 = \omega$ ($t = t_0$) and rotor angle $\delta_0 = \delta$ ($t = t_0$) at the synchronization instant. The running system is assumed to have constant voltage (U) and frequency (ω_s).

The SG is characterized by its d-axis subtransient (X''_d) and transient (X'_d) reactance, the step-up generator transformer by its internal impedance (X_T), and the running system by its equivalent impedance (X_s).

Once the CB is closed at $t = t_0$, the SG is pulled into synchronism with the running system. The machine's dynamics is governed by the swing or motion equation, consisting of the following second-order, non-linear differential equation:

$$2 \cdot H \cdot \frac{d(\omega - \omega_s)}{dt} = 2 \cdot H \cdot \frac{d^2\delta}{dt^2} = T_m - T_e - D \cdot \frac{d\delta}{dt} = T_m - T_e - D \cdot \omega \tag{1}$$

In Equation (1), H denotes the SG's inertia constant; D denotes the damping coefficient accounting for the mechanical losses and the effect of the damper winding, if any; T_m represents the mechanical torque provided by the prime mover; and T_e corresponds to the developed electromagnetic torque.

The analytical expression for the instantaneous electromagnetic torque and its maximum value [12,18–20], experienced by the machine during the faulty synchronization event, are presented in Equations (2) and (3), respectively. For simplicity purposes, from now on, the SG and system voltage magnitudes will be considered similar ($V \approx U$, typically 1 p.u.), easily ensured by any modern synchronizing system. The electromagnetic torque peak achieves its highest magnitude with a phase difference of $\delta_0 = 120°$. This peak is approximately 30% higher than that during a faulty counterphase synchronization ($\delta_0 = 180°$). The resulting torque magnitudes can more than double those during a three-phase terminal short circuit.

$$T_e \approx \frac{U^2}{X''_d + X_T + X_S} \cdot \left[sin\delta_0 - 2 \cdot sin\frac{\delta_0}{2} \cdot cos\left(\omega(t) \cdot t + \frac{\delta_0}{2} \right) \right] \tag{2}$$

$$T_{e,max} \approx \frac{U^2}{X''_d + X_T + X_S} \cdot \left[sin\delta_0 + 2 \cdot sin\frac{\delta_0}{2} \right] \tag{3}$$

After synchronization, ω and δ experience the transient evolution imposed by Equation (1) until the incoming system is pulled into synchronism with the running system once the equilibrium is achieved. The transient evolution may be composed of several torque components applied to the shaft. The steady-state value for ω corresponds to ω ($t = \infty$) $= \omega_s$, i.e., the rotor speed equals the synchronous speed. Usually, as the only active power required from the machine is that necessary to overcome the mechanical losses (the active power setpoint is generally zero), the rotor angle achieves its steady-state value near zero, δ ($t = \infty$) ≈ 0, i.e., the rotor is pulled in phase with the grid voltage.

The system transient derived from the faulty synchronization results in high-magnitude currents after connection, which produce the mentioned high subsequent accelerating or decelerating torques. The transient currents are characterized by an asymmetrical evolution [18,20], consisting of an AC current component, expressed by Equation (4), along with a DC component that attenuates over time, expressed by Equations (5) and (6).

$$i_{AC} \approx \frac{2 \cdot U}{X'_d + X_T + X_S} \cdot sin\frac{\delta}{2} \tag{4}$$

$$i_{DC} \approx \frac{2 \cdot U}{X_d'' + X_T + X_S} \cdot sin\frac{\delta_0}{2} \cdot e^{-\frac{t}{\tau}} \tag{5}$$

$$\tau = \frac{\frac{1}{2}\left(X_d'' + X_q''\right) + X_T + X_S}{R_G + R_T + R_S} \cdot \frac{1}{\omega_s} \tag{6}$$

As per Equation (4), the AC current component is quickly reduced by the change in rotor angle δ. Nevertheless, high initial rotor angles δ_0 imply larger current asymmetries. The attenuation of such asymmetry is intimately related to the circuit time constant (τ), defined as the inverse of the decay rate (*R/X* ratio). The time constant defined by Equation (6) accounts for the SG's d-axis (X_d'') and q-axis (X_q'') subtransient reactance, for X_T and X_S on the inductive side, and for the corresponding values for the SG, transformer, and system (R_G, R_T, and R_S) on the resistive side.

It should be noted that the decay rate is related to the SG's and transformer's impedance transient behavior (from subtransient to transient and from transient to synchronous). If the DC component decay rate is excessively long, current zero-crossings can be delayed for several cycles, thus postponing the current interruption by the CB [18].

2.2. Voltage Magnitude Mismatch

A magnitude discrepancy between the SG and system voltage ($V \neq U$) leads to reactive power flow after the CB closing. The quantification of the initial var-flow (Q) is given by Equation (7). Evidently, this var-flow ceases once the SG terminal voltage is imposed by the running system after synchronization.

$$Q \approx \frac{3 \cdot U}{X_d'' + X_T + X_S} \cdot [V \cdot cos\delta_0 - U] \tag{7}$$

If the SG's per-unit voltage is lower than that of the interconnected system ($V < U$), the machine will absorb reactive power from the running system. This interaction may induce a voltage sag in the power system, instigating system voltage instability. The increased reactive power demand may cause a greater voltage drop across the connecting lines, potentially leading to uncontrollable drops and, ultimately, system collapse. This issue is especially concerning in electrically weak systems or those lacking sufficient local reactive power support.

According to standards for salient-pole [21] and cylindrical rotor SGs [22], the machines must be designed to withstand a voltage magnitude mismatch of $\Delta U_0 = +5\%$ during synchronization. This specification considers the SG's rated voltage as the reference, implying that the SG's induced voltage should be higher than the voltage of the running system immediately before synchronization. Therefore, proper excitation control should be performed by the synchronizer in order to ensure that the SG's electro-magnetomotive force magnitude is just above the system voltage magnitude before synchronization.

2.3. Phase Angle Mismatch

As derived from Section 2.1, significant phase angle mismatch between the electro-magnetomotive force delivered by the SG and the running system voltage ($\delta_0 \neq 0$) can result in high-magnitude currents after interconnection, with consequently high electrical transients and subsequent accelerating ($\delta_0 > 0$, i.e., the incoming system leads) or decelerating torque ($\delta_0 < 0$, i.e., the incoming system lags).

The transient current resulting from a faulty synchronization, assuming ideally aligned frequency across the CB ($\omega_0 = \omega_s$), can be expressed in the phasor form as per Equations (8) and (9) [23,24]. In Equations (8) and (9), $\underline{V} = V_{<\delta0>}$ and $\underline{U} = U_{<0>}$ correspond to the SG terminal and power system voltages, respectively, while $Z = R + j \cdot X$ designates the total impedance that limits the fault current (mainly the generator subtransient reactance, the step-up transformer impedance, and the power system impedance). An

asymmetrical factor, K_{asym}, is employed to account for the DC component within the transient fault current.

$$\underline{I} = \frac{V - U}{Z} \cdot K_{asym} = \frac{V_{\langle \delta_0 \rangle} - U_{\langle 0 \rangle}}{Z} \cdot K_{asym} \tag{8}$$

$$K_{asym} = \sqrt{2} \cdot \left[1 + \left(e^{-(arctan \frac{X}{R} + \frac{\pi}{2}) \cdot \frac{R}{X}} \right) \cdot sin \left(arctan \frac{X}{R} \right) \right] \tag{9}$$

From Equation (8), if similar SG and system voltages are assumed at 1 p.u. ($V \approx U \approx 1$ p.u.), the voltage across the CB can reach up to 2 p.u. when the rotor angle at the synchronization instant is $\delta_0 = 180°$. This is the worst-case scenario maximizing the current components in Equations (4) and (5). Such out-of-phase synchronizations imply high currents that can largely exceed that of a three-phase solid short circuit at the SG terminals, which is the event for which the stator windings and the transformers are usually designed for [1].

In this regard, excessive phase angle differences can not only lead to winding overheating but also to considerable mechanical effects, such as winding deformation, or even winding failure under an occasional or fatigue failure mode. In fact, out-of-phase synchronizations expose the SG and the coupled drive to dangerous mechanical transient torques. In accordance with Equation (1), after an out-of-phase synchronization, the rotor is rapidly accelerated or decelerated in order to pull in the SG voltage in phase with the running system voltage. For example, if the incoming system voltage leads the running system voltage ($\delta_0 > 0$), the electromagnetic torque given by Equation (2) pulls the rotor in a braking action ($T_e > 0$) in opposition to the rotating momentum so as to reduce the rotor angle. This means that the rotor is initially decelerated in the transient period ($d\omega/dt < 0$). The opposite situation occurs if the incoming system voltage lags the running system voltage ($\delta_0 < 0$).

The oscillating electromagnetic torque [16] is produced following the mechanical dynamics expressed in Equation (1) until the steady-state conditions are achieved. The process comprises several deceleration and acceleration periods. The SG's inertia determines the number of torque oscillations required to pull in the generator in alignment with the system. The decaying of these transients is related to the system damping upon synchronization, which under no-load conditions is not so significant. As long as the machine does not step out of the stability region throughout the process, $\delta \, (t = \infty) \approx 0$ is generally achieved at the steady state, i.e., the running and incoming systems are aligned in angle. This is generally true given that the synchronization is usually performed at no-load conditions, i.e., the prime mover only provides limited torque to overcome shaft mechanical losses.

According to standards for salient-pole [21] and cylindrical rotor SGs [22], synchronization should be performed with phase angle mismatches less than $\Delta\delta_0 = \pm 10°$ to avoid the described electrical and torsional stresses. Therefore, accurate synchronization techniques should be employed, considering the CB closing delay, among other factors.

2.4. Frequency Mismatch

The slip frequency, defined as the difference between the incoming and running systems frequencies before synchronization, is another cause of electrical and mechanical stress. After a synchronization with high slip frequency, the rotor is rapidly accelerated (if $\omega_0 < \omega_s$) or decelerated (if $\omega_0 > \omega_s$), with the corresponding dynamics described by Equations (1) and (2), in order to pull in the SG in synchronism with the system, similarly as in out-of-phase synchronizations.

Indeed, frequency mismatches necessarily imply phase angle discrepancies at each moment. Therefore, the dynamics are similar to those developed for out-of-phase synchronizations. For example, if the incoming system runs faster than the power system ($\omega_0 > \omega_s$), the electromagnetic torque given by Equation (2) initially pulls the rotor in a braking action ($T_e > 0$ and $d\omega/dt < 0$) opposite to the rotating momentum so as to reduce the slip frequency and vice versa if the incoming system runs slower than the power system ($\omega_0 < \omega_s$).

Analogously to out-of-phase synchronizations, the final state is achieved at the synchronism speed ($\omega \, (t = \infty) = \omega_s$), i.e., the running and incoming systems are aligned in

speed. The SG's inertia determines the total number of torque oscillations that are required to pull in the generator in synchronism with the system. If the slip frequency is large enough, multiple slip cycles may be induced before the SG's speed matches the system's speed. Each slip cycle causes an out-of-phase current to flow through the stator windings.

According to standards for salient-pole [21] and cylindrical rotor SGs [22], synchronization should be performed with a slip frequency less than $\Delta f_0 = \pm 0.067$ Hz to avoid high electrical and torsional stresses. It should be noted that phase angle mismatches as low as $\delta = 15°$ can cause power swings equivalent to slip frequencies of 0.5 Hz, which is considerably higher than the prescribed limit. Moreover, it can be demonstrated that the slip frequency does not have a significant effect on the produced electromagnetic torque [1] when an out-of-phase synchronization is conducted. Thus, the impact of out-of-phase synchronizations alone is relatively worse than the impact of synchronizations with slip frequency alone, although the combined effect of both is a usual cause of fatigue failure, as the slip frequency leads to a greater need for swing cycles before the SG aligns its speed with that of the system.

2.5. A Common Cause of Faulty Synchronizations in the Industry

While manual and automatic synchronization systems are effective at ensuring that voltage magnitude and frequency are aligned, achieving actual phase angle equality relies on the correct wiring of the VTs circuits and the synchronization equipment circuits during commissioning or maintenance. An example of a correct wiring is shown in Figure 2. Any wiring error, as long as it is not coincidentally compensated by another error, can result in phase angle mismatches of $\delta = \pm 60°$, $\pm 120°$, or $\pm 180°$, as illustrated in Figures 3 and 4. These mismatches occur because incorrect wiring can cause the synchronization system to receive inaccurate phase information, leading to erroneous timing of the CB closing. Therefore, among all possible faulty synchronization issues, out-of-phase synchronizations are the most common.
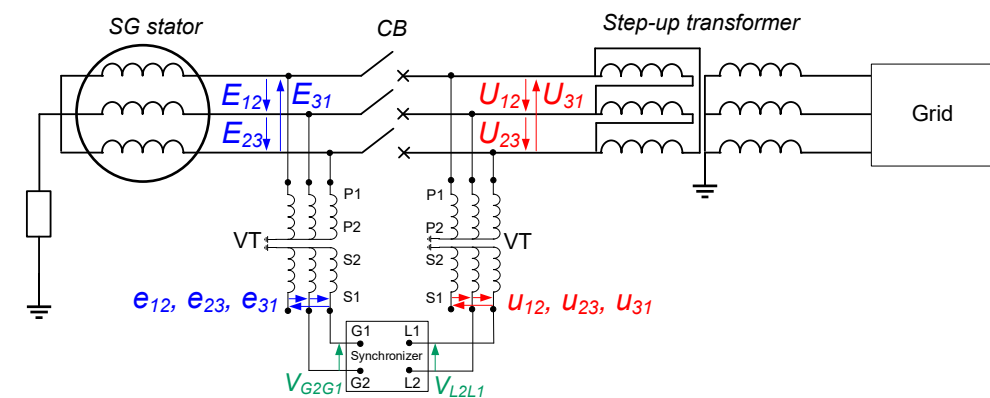
Figure 2. An example of the correct wiring of a VT and synchronizer, with detail of all the voltages.

Following the examples of erroneous wirings shown in Figure 3, the phasor constructions featuring the VTs' secondary-side line-voltage values ($\underline{e}_{12}$, $\underline{e}_{23}$, and $\underline{e}_{31}$ for the machine-side VT; $\underline{u}_{12}$, $\underline{u}_{23}$, and $\underline{u}_{31}$ for the system-side VT) are shown in Figure 4. The synchronizer (ANSI 25) ensures zero-phase shift between voltages $\underline{v}_{G2G1}$ and $\underline{v}_{L2L1}$. These voltages depend on the wirings of the VTs and the synchronizer. Any error in these wirings may imply that $\underline{v}_{G2G1}$ and $\underline{v}_{L2L1}$ being in phase mean an actual phase shift between the voltages across the CB, thus a non-zero rotor angle.

Several examples are shown in Figures 3 and 4: F1, swapped wiring on one side of the input to the synchronizer ($\delta_0 = 180°$, i.e., counterphase synchronization); F2, phase swap at the primary side of a VT ($\delta_0 = 180°$, i.e., counterphase synchronization); and F3 and F4, erroneous phase combinations on one side of the input of the synchronizer ($\delta_0 = 120°$ and $\delta_0 = 60°$, respectively).
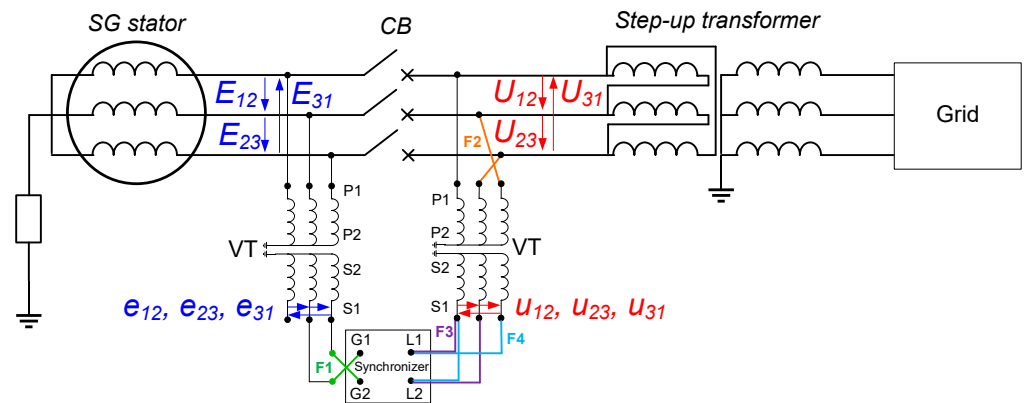
Figure 3. Incorrect wirings (F1: swapped wiring on one side of the synchronizer; F2: phase swap at the primary side of a VT; and F3 and F4: erroneous phase wirings on the secondary side of a VT).
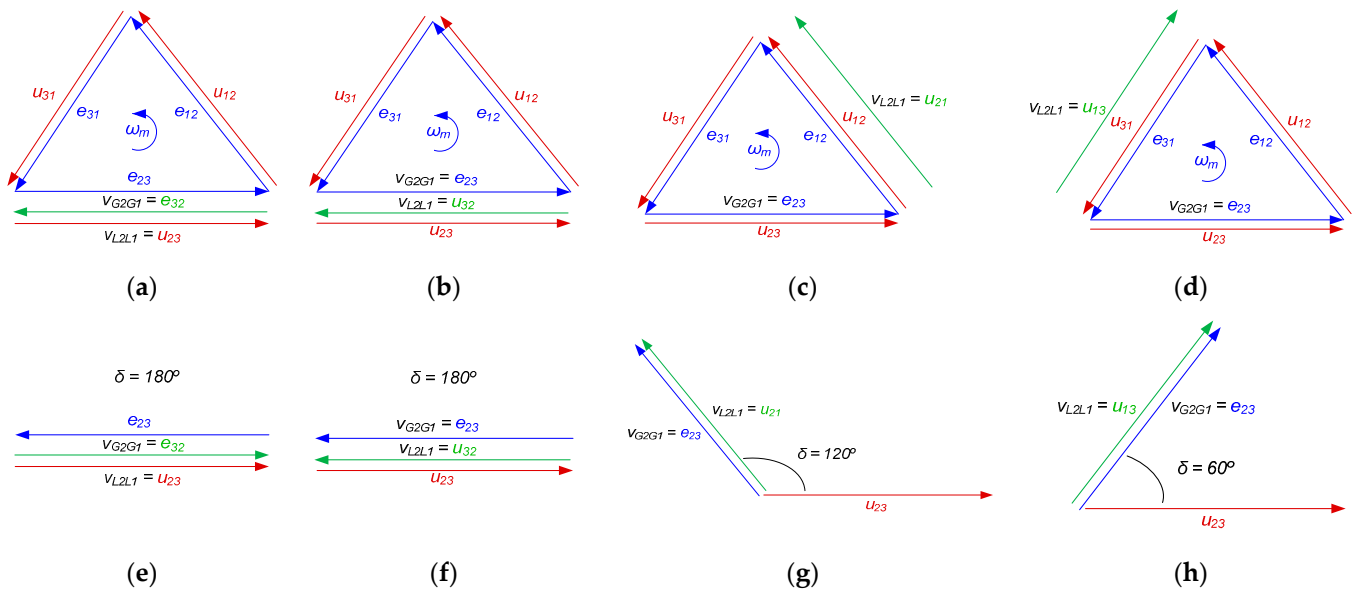
Figure 4. Out-of-phase synchronization conditions due to wiring errors [(**a**), (**b**), (**c**), and (**d**): general phasor construction for faults F1, F2, F3, and F4, respectively; (**e**), (**f**), (**g**), and (**h**): specific phasor construction at the synchronization instant for faults F1, F2, F3, and F4, respectively].

Out-of-phase synchronizations have been widely reported as a critical issue in the power generation industry [10–12]. Mechanical impacts on the SG due to excessively high instantaneous currents and transient torques can include loosening of the stator winding bracing and blocking as well as deformation, cumulative fatigue damage, or even cracking of coupling bolts, couplings, and rotor shafts. The impulse current may also compromise the integrity of the winding insulation, potentially leading to insulation breakdown. Furthermore, the magnetic flux density can become saturated at the rotor pole surface, which increases the stress on the rotor teeth and may lead to localized overheating and mechanical fatigue. These conditions can significantly shorten the operational lifespan of the SG and, in extreme scenarios, result in catastrophic failures. In addition to affecting the SG itself, the transient conditions induced by out-of-phase synchronizations can also adversely impact the prime mover and the generator transformer windings.

3. Protection for Faulty Synchronizations

3.1. Behavior of Conventional SG Protection Functions in the Case of Faulty Synchronization

On the one hand, although detecting faulty synchronizations is not their purpose, there are some conventional SG protection functions [25] that are theoretically sensitive to

faulty synchronizations according to their operational principles. However, due to their usual settings, these protection functions do not usually activate in practice, or if they eventually do, it occurs after excessively long time delays. These protection functions are analyzed in the following points.

(a) The reverse power protection (ANSI 32) may detect out-of-phase or high-slip synchronizations, as these conditions can lead to transient real power absorption from the power system while attempting to bring the machine into synchronism. However, even if the reverse power protection element detects the transient power flow, the time delays associated with this element typically prevent it from initiating a trip response. The reverse power condition resulting from a faulty synchronization is usually too brief to activate a trip.

(b) Loss-of-field protection (ANSI 40) can be activated by the transient reactive power flow caused by significant voltage magnitude variations if the protective element is set with high sensitivity and a short time delay, which is not generally the case, as detecting such conditions is not its purpose.

In fact, the standard practice involves synchronizing with a slightly positive slip and ensuring that the generator voltage is marginally higher than the bus voltage in order to help prevent the eventual activation of reverse power (ANSI 32) and loss-of-field (ANSI 40) protections, respectively.

(c) Overcurrent protection (ANSI 51) does not activate instantaneously because SGs are required to supply a certain overcurrent without disconnecting from the grid during external short circuits, as this element functions as a backup protection for external faults. Therefore, this protection leads to an excessively delayed tripping response in the case of faulty synchronizations.

(d) Under-impedance protection (ANSI 21) may activate according to its operational principle, but as it is commonly employed as backup protection for both external and internal faults, triggering is not quick enough to mitigate potential damage related to faulty synchronizations.

Conversely, other conventional SG protection functions are unable to detect faulty synchronizations. Differential protection (ANSI 87G) typically does not activate in such cases because there is no current difference between the two sides of the stator or the step-up transformer windings. Similarly, stator-ground fault protection (ANSI 51N or 59N) is not triggered, as no ground current is involved. Pole slip or out-of-step protection (ANSI 78) usually does not activate because the mechanical power provided by the prime mover is generally insufficient to cause asynchronous operation of the SG at synchronization. Lastly, inadvertent energization protection, which combines instantaneous overcurrent protection (ANSI 50) and undervoltage protection (ANSI 27), is typically only active when the SG is not in operation (either at standstill condition or on turning gear) and is disabled once the SG's output voltage reaches approximately 80% of its rated value. Consequently, this protection is also unable to detect faulty synchronizations.

When a faulty synchronization occurs, the transient overcurrent may persist for several cycles or even several seconds until some of the conventional protection relays activate. Generally, the under-impedance relay would operate first, as it usually has the fastest setting among the protection functions that can detect faulty synchronizations [10]. However, it has been reported that differential protections can also misoperate due to current transformer (CT) saturation [12].

3.2. Developments in Protection Methods for Faulty Synchronizations

Advancements in SG synchronization have primarily focused on modern automatic synchronizers (autosynchronizers) and synchronism-check relays [26]. Recent research has addressed SG control topics, including control for the coordinated synchronization of SGs [27], synchronizations under grid frequency instability [28], paralleling of SGs and virtual SGs [29], and SG paralleling under a leader–follower approach [30].

As introduced in Section 1, on the one hand, the advancements in autosynchronizers [31–36] improve synchronization precision by automatically controlling the SG's voltage and frequency, avoiding human errors and ensuring parameter alignment (voltage magnitude, phase angle, and frequency). On the other hand, the synchronism-check relay [37] serves as ultimate safeguard by blocking the CB while the synchronization conditions are not achieved.

However, as noted in [26], the literature lacks comprehensive protection schemes to address all potential contingencies. Autosynchronizer and synchronism-check technologies aim to prevent these contingencies but not provide any kind of protection once a contingency occurs. Among the contingencies listed in Section 1, wiring errors are particularly critical, as described in Section 2.5. When a wiring error exists and affects the autosynchronizer or the synchronism-check relay, these systems may receive incorrect phase information. Even if functioning correctly, these systems will lead to the CB closing based on erroneous phase data, resulting in an out-of-phase synchronization despite appearing in phase. Consequently, these technologies are ineffective in the presence of contingencies, underscoring the need for dedicated protection schemes to promptly detect and address faulty synchronizations.

Without a dedicated synchronization protection function capable of tripping the machine immediately in the event of faulty synchronizations, the transient overcurrent may persist for several cycles or even several seconds. This can often lead to severe damage to the SG, the prime mover, and associated power equipment as well as significant disruptions to the power system.

For over two decades, dedicated alarming and tripping mechanisms for out-of-phase synchronizations have relied on overcurrent protection schemes [10,12,20], which are armed by either the CB status (the overcurrent element is activated after the CB is closed) or the line current (the overcurrent element is activated after another lower-set overcurrent element picks up for any loaded scenario). These schemes are typically activated for a duration of 15 cycles [12,20] or an adjustable dropout time delay [10]. When configured for alarming, the pickup setting is generally set at low current values (usually < 1 p.u.), which correspond to low synchronizing angles (commonly $\delta_0 < 60°$). Conversely, when configured for tripping, the threshold is typically set higher, taking into account the interruption capacity of the CB and analyzing the zero-crossings of the current waveform. For instance, according to Equation (4), a threshold of 3.5 p.u. for $\delta_0 = 60°$ is advisable, representing a practical trade-off value. Moreover, care must be taken in case of black-start, as the inrush current resulting from transformer energization can be higher than the threshold of the overcurrent element [1]. In these cases, an additional dead-bus close permissive condition should be added to provide security to the scheme.

These overcurrent schemes provide unambiguous targeting associated with out-of-phase synchronizations. Furthermore, these schemes can be easily implemented using the programmable logic of conventional relays. Eventually, this implementation can be carried out by modifying the inadvertent energization function through the deactivation of voltage supervision.

The main problem of the aforementioned overcurrent schemes is their reliance on RMS values, which necessarily introduces a calculative delay due to the time required for RMS computation, often several cycles. This notably delays fault detection, which can be greatly detrimental, as the initial cycles following CB closing during a faulty synchronization can inflict severe damage due to extreme electrical transients and elevated electromagnetic torque.

The method proposed herein enhances the dedicated detection capabilities by utilizing instantaneous current measurements and their derivatives, enabling quicker response times. This approach significantly mitigates the lag associated with traditional RMS-based calculations, providing a critical advantage over existing methods at safeguarding equipment during potentially hazardous synchronization events.

However, the main limitation of the proposed method is that its applicability is contingent to the utilization of instantaneous value relays, which are not as generalized as RMS value relays that are commonly employed in the industry. Although significantly improving the fault detection time, fault clearance remains dependable on the limitations of switchgear, mainly the CB location, breaking capacity, opening time, and pole scatter. It should be also noted that the proposed protection scheme is not a replacement for commissioning practices, including the verification of synchronizing circuits, as avoiding the occurrence of faulty synchronizations is the first line of defense.

4. Principles of the Proposed Protection

During a normal synchronization of an SG, immediately after the generator CB is closed, synchronization currents as low as 0.3–0.5 p.u. flow. This current flow can be due to various reasons:

- Differences in the voltage magnitude, frequency, and phase angle (within the limits prescribed by standards, manufacturers, and regulations);
- CB pole scatter;
- Residual generator magnetization;
- Load sharing or generator paralleling;
- Auxiliary service consumption;
- Voltage drops due to non-ideal system impedances;
- Governor and AVR control fine adjustments, among other factors.

Once the CB is closed, the operation modes shifts from speed and voltage control to active and reactive power control through the governor and the AVR, respectively. The active and reactive power setpoints are usually close to zero after synchronization; thereby, the currents achieve their steady state close to zero within a few cycles. Afterwards, the usual practice involves increasing the active and reactive power setpoints to the desired operating point.

In contrast, in the case of a faulty synchronization, due to voltage magnitude, frequency, or phase angle mismatches, the magnitude of the currents largely exceeds that of a normal synchronization. The magnitude of these currents is related to the deviations present at the synchronization instant. For instance, from Equation (4), it is derived that the value of i_{AC} is a function of δ impacted by the initial rotor angle δ_0 just after synchronizations—δ evolving afterward according to the dynamics reflected in Equation (1)—and from Equation (5), it is derived that i_{DC} is directly impacted by the initial rotor angle δ_0. In some cases, faulty synchronizations can result in currents significantly exceeding those of a three-phase terminal short circuit.

Additionally, from Equations (4) and (5), the time derivative of the current can be computed, as shown in Equation (10), and particularized at $t = t_0$, as in Equation (11). In Equation (11), the absolute value of the total current derivative increases for larger values of δ_0. It should be noted that the first time derivative of the rotor angle δ is governed by the swing equation, which reflects the imbalance between mechanical and electrical power, as shown in Equation (1). Larger values of δ_0 correspond to a larger initial displacement, leading to higher rates of change in the oscillatory behavior of δ. This dynamic is driven by the electromagnetic torque, described in Equation (2), which depends on terms involving $sin\,\delta_0$ and $sin\,(\delta_0/2)$. The time derivative of the AC component attenuates over time as δ approaches zero, while the DC component attenuates over time according to the decay ratio.

$$\frac{di}{dt} = \frac{d}{dt}[i_{AC} + i_{DC}] \approx \frac{U}{X'_d + X_T + X_S} \cdot \cos\frac{\delta}{2} \cdot \frac{d\delta}{dt} - \frac{2 \cdot U}{\tau \cdot (X''_d + X_T + X_S)} \cdot \sin\frac{\delta_0}{2} \cdot e^{-\frac{t}{\tau}} \quad (10)$$

$$\left.\frac{di}{dt}\right|_{t \approx t_0} \approx \frac{U}{X'_d + X_T + X_S} \cdot \cos\frac{\delta_0}{2} \cdot \left.\frac{d\delta}{dt}\right|_{t \approx t_0} - \frac{2 \cdot U}{\tau \cdot (X''_d + X_T + X_S)} \cdot \sin\frac{\delta_0}{2} \cdot e^{-\frac{t_0}{\tau}} \quad (11)$$

The proposed method leverages the principle that the current and the current-derivative values attain higher values in the case of faulty synchronizations compared to normal syn-

chronizations. The method introduces a novel protective approach to faulty synchronizations of SGs based on an overcurrent scheme ($i>$) and a current-derivative ($di/dt>$) scheme that rely on instantaneous current values, which are activated during the synchronization process.

The protective scheme triggers a tripping signal when the measured instantaneous current exceeds a certain threshold (i_{SET}) and/or when the current-derivative value exceeds the corresponding threshold (di/dt_{SET}) during the protection activation period ($t_0 < t < T_{SET}$), as indicated in Equations (12) and (13), respectively.

To ensure the reliability of the method under any operational condition, a tripping delay (ε) can be included in Equations (12) and (13). This delay requires the tripping conditions to be consistently met over the specified duration before protection is triggered. To avoid spurious triggering, this time delay should be set appropriately exceeding the characteristic period of high-frequency noise observed in field applications.

$$|i[t; t+\varepsilon]| > i_{SET} \rightarrow Trip \tag{12}$$

$$\left|\frac{di}{dt}[t; t+\varepsilon]\right| > \frac{di}{dt}_{SET} \rightarrow Trip \tag{13}$$

The setting of the instantaneous overcurrent threshold (i_{SET}) should be adjusted above the peak current value for a normal synchronization. This threshold can be calculated by particularizing $i_{AC} + i_{DC}$, derived from Equations (4) and (5), for $t = t_0 \approx 0^+$ and $\delta = \delta_0$ and replacing δ_0 with the maximum admissible phase angle mismatch. The setting of the instantaneous current-derivative threshold (di/dt_{SET}) should be set above the peak current-derivative value for a normal synchronization. This threshold can be calculated by particularizing Equation (11) for $t = t_0 \approx 0^+$, resorting to Equations (1) and (2) for the dynamics of δ. The protective schemes are enabled shortly before the synchronization instant ($t = t_0$) and are disabled after an adjustable time delay (T_{SET}) prior to increasing the power output.

In the proposed method, the thresholds (i_{SET}, di/dt_{SET}, and T_{SET}) should be set according to an initial healthy reference synchronization performed prior to protection commissioning. In this synchronization, key parameters (voltage magnitude, frequency, and phase angle differences) should be kept within the tolerance windows defined by standards, regulations, or manufacturer specifications, typically using the most restrictive values. Since synchronization is a routine operation in power generation plants, this approach is practical and ensures that the tripping thresholds are accurately and reliably set based on an actual healthy synchronization.

However, if during the whole activation time interval the current derivative remains below the threshold, the protective scheme is disabled at $t = T_{SET}$, and the active and reactive power setpoints are increased to the desired operating point. Therefore, the coordination of this parameter with the governor and the AVR is required. A theoretical representation of the method is provided in Figure 5. The logical layout of the proposed protective scheme is illustrated in Figure 6.

The proposed protective schemes offer faster fault detection compared to the state-of-the-art overcurrent algorithms for the same application [10,12,20], as the scheme is not based on various RMS currents but on instantaneous current measurements. By reducing the fault detection time, earlier fault clearance can be achieved, mitigating the duration of the associated electrical and mechanical stresses on the SG and minimizing stability issues within the power system.

In practice, the current derivative can be calculated by means of the rate of change of current, as in Equation (14), given two instantaneous current measurements (i_1 and i_2 at times t_1 and t_2, respectively, with $t_1 < t_2 < T_{SET}$). In Equation (14), $t_2 - t_1$ corresponds to the sampling period (T).

$$\frac{di}{dt}(t) \approx \frac{\Delta i}{\Delta t}(t) = \frac{i_2 - i_1}{t_2 - t_1} \tag{14}$$
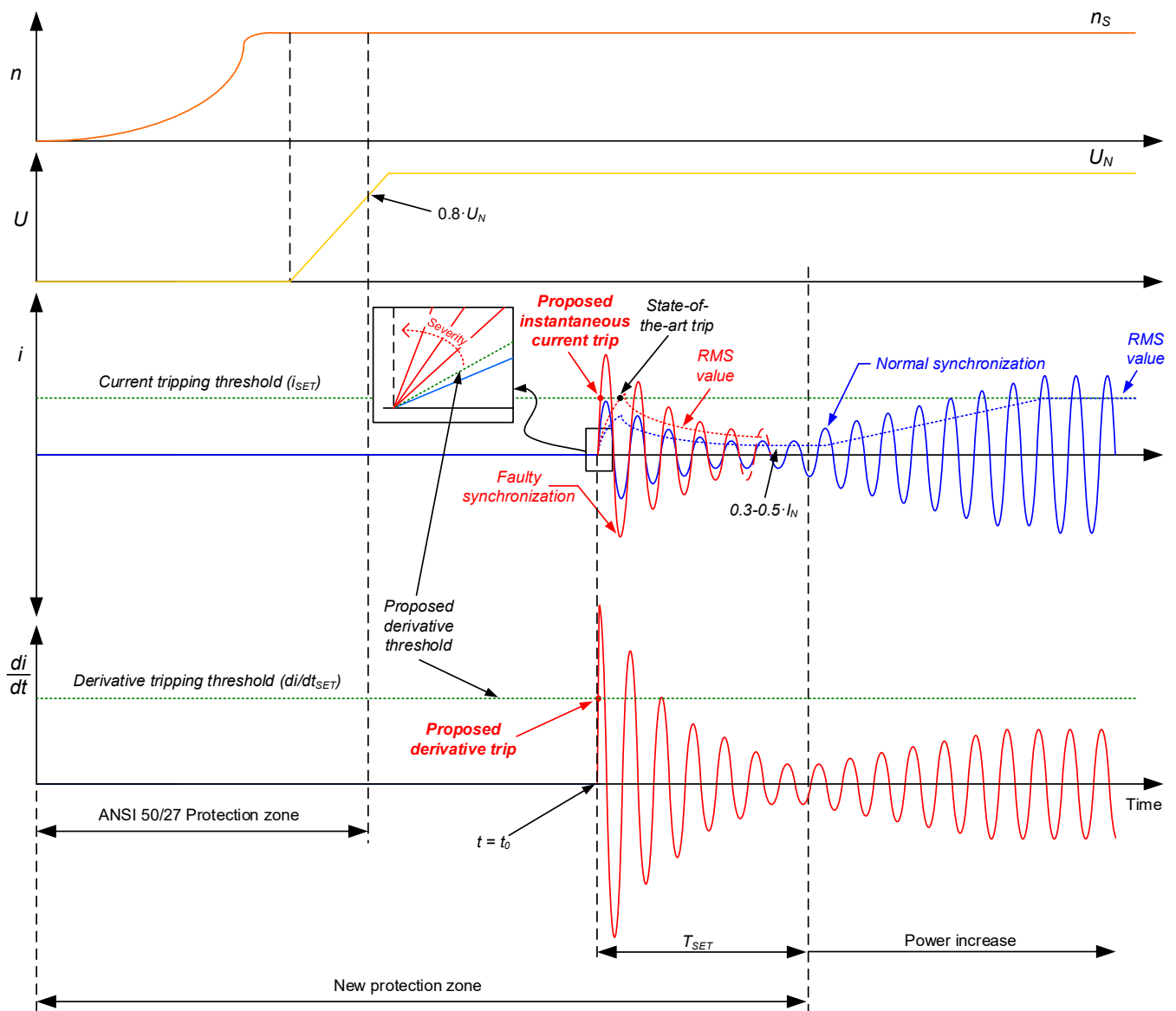
Figure 5. The theoretical representation of the proposed protection method (*n*: rotor speed; *U*: stator voltage; *i*: stator current; *di/dt*: stator current derivative).
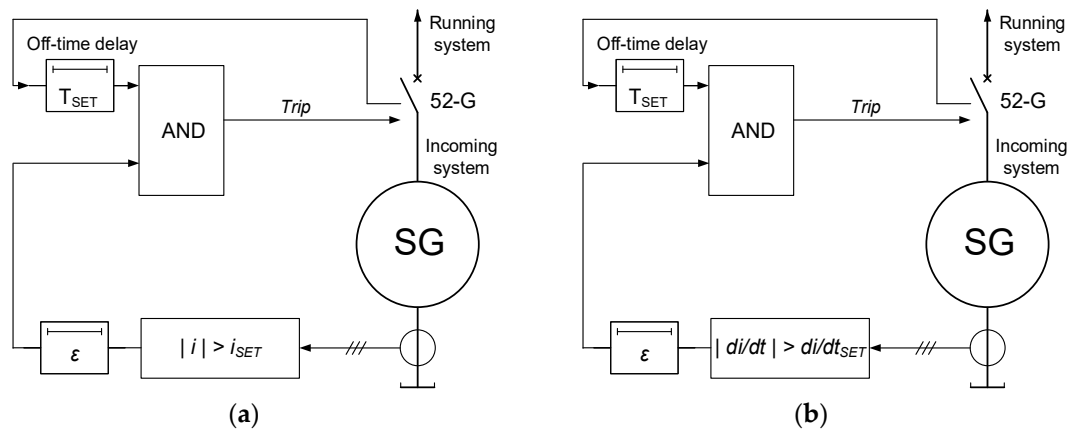
Figure 6. The schematic layout of the proposed protective scheme: (**a**) instantaneous current value scheme; (**b**) instantaneous current-derivative value scheme.

Alternatively, in addition to the introduction of the tripping delay (ε), further measures can be adopted to avoid measurement noise or calculation glitches and, more importantly, to lighten the computational burden of the method. Sampling can be improved by calculating the average value from multiple instantaneous current measurements uniformly distributed within the original sampling period T, as expressed in Equation (15). Similarly, the current-derivative approach can be improved, as expressed in Equation (16). A batch of instantaneous current measurements $\{i_1,\ldots, i_j,\ldots, i_{N+1}\}$ are taken within T for the calculation, with N being the number of uniform segments in which the sampling period is divided into. It should be noted that Equation (16) is a particularization of Equation (14) for $N = 1$.

$$i = \frac{N}{T} \cdot \sum_{j=1}^{N+1} i_j \tag{15}$$

$$\frac{di}{dt} \approx \frac{\Delta i}{\Delta t} = \sum_{j=1}^{N+1} \frac{i_{j+1} - i_j}{\frac{T}{N}} = \frac{N}{T} \cdot \sum_{j=1}^{N+1} \left(i_{j+1} - i_j \right) \tag{16}$$

The proposed per-batch average calculation effectively dampens noise and derivative calculation glitches. However, it requires measuring devices with a sampling frequency of N/T. Optimal values for parameters T and N must be carefully selected considering the limitations of the measuring devices. If T is too small, the method may become overly sensitive to noise or glitches, increasing the risk of false triggering. Conversely, an excessively large T could reduce dependability, delaying fault detection. The parameter N should be set according to T, ensuring enough samples are collected within T to minimize the impact of peaks due to noise or glitches on the average value.

5. Computer Simulations

5.1. Simulation Model

The proposed simulation model, developed in MATLAB-Simulink®, is designed to analyze the protection mechanism for faulty synchronizations of an SG with the power grid. The model shown in Figure 7 illustrates a 362 MVA SG connected to a 400 kV transmission grid through a 400/18 kV step-up transformer rated at 362 MVA.
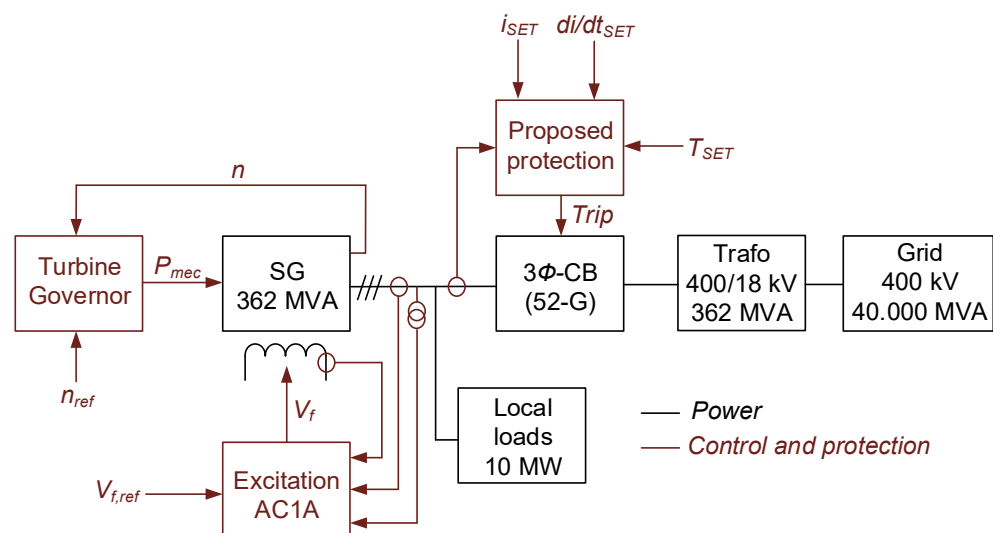
Figure 7. The schematic layout of the simulation model.

The SG (Table 1) is of cylindrical type, with stator winding connected in Wye to an internal neutral point. The machine is modeled in the dq-reference frame. The SG is driven by a turbine governor (Table 2), which regulates the mechanical power input (P_{mec}) based

on reference speed (n_{ref}). The expressions of the controller and actuator transfer functions utilized in the turbine governor block are given in Equations (17) and (18), respectively.

$$H_c(s) = K \cdot \frac{1 + T_3 \cdot s}{1 + T_1 \cdot s + T_1 \cdot T_2 \cdot s^2} \tag{17}$$

$$H_a(s) = \frac{1 + T_4 \cdot s}{s \cdot (1 + T_5 \cdot s) \cdot (1 + T_6 \cdot s)} \tag{18}$$

Table 1. Data of the SG used in the simulation model.

Magnitude	Value	Units
Rated apparent power (S_n)	362	MVA
Rated power factor (PFn)	0.8	
Rated voltage (U_n)	18	kV
Rated frequency (f_n)	50	Hz
Rated speed (n_n)	3000	rpm
D-axis synchronous reactance (X_d)	2.580	p.u.
Q-axis synchronous reactance (X_q)	2.505	p.u.
D-axis transient reactance (X'_d)	0.455	p.u.
Q-axis transient reactance (X'_q)	0.500	p.u.
D-axis subtransient reactance (X''_d)	0.313	p.u.
Q-axis subtransient reactance (X''_q)	0.348	p.u.
Leakage reactance (X_l)	0.278	p.u.
D-axis transient short-circuit time const. (T'_d)	1.11	s
D-axis subtransient short-circuit time const. (T''_d)	20	ms
Q-axis transient open-circuit time const. (T'_q)	1.04	s
Q-axis subtransient open-circuit time const. (T''_q)	35	ms
Stator resistance (R_s)	0.002	p.u.
Rated field current (I_{fn})	2803	A
Rated field voltage (V_{fn})	492	V
Inertia coefficient ($H(s)$)	1.058	

Table 2. Data of the turbine governor used in the simulation model.

Magnitude	Value	Units
Regulator gain (K)	40	
Regulator time const. T_1	0.01	
Regulator time const. T_2	0.02	
Regulator time const. T_3	0.20	
Actuator time const. T_4	0.25	
Actuator time const. T_5	0.009	
Actuator time const. T_6	0.0384	
Engine time delay (T_d)	24	ms

The excitation system (Table 3) corresponds to an adaptation of the AC1A excitation system of the IEEE 421 standard [38], which adjusts the field voltage (V_f) based on the reference voltage ($V_{f,ref}$). The excitation block models an AC alternator driving a diode rectifier to produce the required field voltage.

The generator output is connected to the power grid via a three-phase CB with negligible pole resistance, and a step-up power transformer (Table 4). The grid (Table 5) is modeled as a 400 kV system with a short-circuit capacity of 40,000 MVA, representing a stiff grid capable of absorbing significant fault currents. The generator also supplies local loads rated at 10 MW, simulating the operational demand of the auxiliary services at the power plant.

Table 3. Data of the excitation system used in the simulation model.

Magnitude	Value	Units
Low-pass filter time const (T_r)	20	ms
Voltage regulator gain (K_a)	400	
Voltage regulator time const. (T_a)	20	ms
Damping filter gain (K_f)	0.03	
Damping filter time const. (T_f)	1	s
Exciter gain (K_e)	1	
Exciter time const (T_e)	0.80	s
Exciter alternator voltage on air-gap line (V_{e1})	4.18	p.u.
Exciter alternator voltage on no-load sat curve (V_{e2})	3.14	p.u.
Exciter saturation voltage on air-gap line (V_{se1})	0.10	p.u.
Exciter saturation voltage on no-load sat curve (V_{se2})	0.03	p.u.
Demagnetizing factor (K_d)	0.38	p.u.
Rectifier loading factor (K_c)	0.20	p.u.

Table 4. Data of the power transformer used in the simulation model.

Magnitude	Value	Units
Rated power (S_n)	362	MVA
Rated frequency (f_n)	50	Hz
Winding connection	YNd11	
Voltage ratio	$400 \pm 15 \times 1\%/18$	kV
Load losses	0.12	%
Non-load losses	0.01	%
Non-load current	0.45	%
Short-circuit impedance	13.05	%

Table 5. Data of the power system used in the simulation model.

Magnitude	Value	Units
Phase-to-phase voltage (U_n)	400	kV
Frequency (f)	50	Hz
Three-phase short-circuit level (S_n)	40,000	MVA
X/R ratio	10	

5.2. Correct Synchronizations

Correct synchronizations were initially conducted by involving two different cases. The first scenario (Case 1) simulated ideal synchronization conditions, with no voltage difference ($\Delta U_0 = 0\%$), no phase angle deviation ($\Delta \delta_0 = 0°$), and a slight frequency difference ($\Delta f_0 = 0.1$ Hz). The second scenario (Case 2) represented synchronization just within the tolerance limits prescribed by technical regulations [39], with a voltage deviation of $\Delta U_0 = 10\%$, a phase angle deviation of $\Delta \delta_0 = 10°$, and a frequency difference of $\Delta f_0 = 0.2$ Hz.

In the most favorable case (Case 1), following the CB closing at $t = 0.1$ s, the current peaks reached approximately 6% of the rated current, as shown in Figure 8a. The current derivative peaked at around 2.8×10^5 p.u./s, as observed in Figure 8b. This indicated a minimal transient response that can be considered negligible. The electromagnetic torque exhibited a small oscillatory behavior, reaching only 8.4% of the rated value, as shown in Figure 8c. The rotor shaft speed settled at the rated value, with the system reaching a steady state approximately 1 s after synchronization, as derived from Figure 8d. These results suggest that a correctly executed synchronization of an SG to the grid leads to minimal transient effects, both on the machine and the grid.

(a)

(b)

(c)

(d)
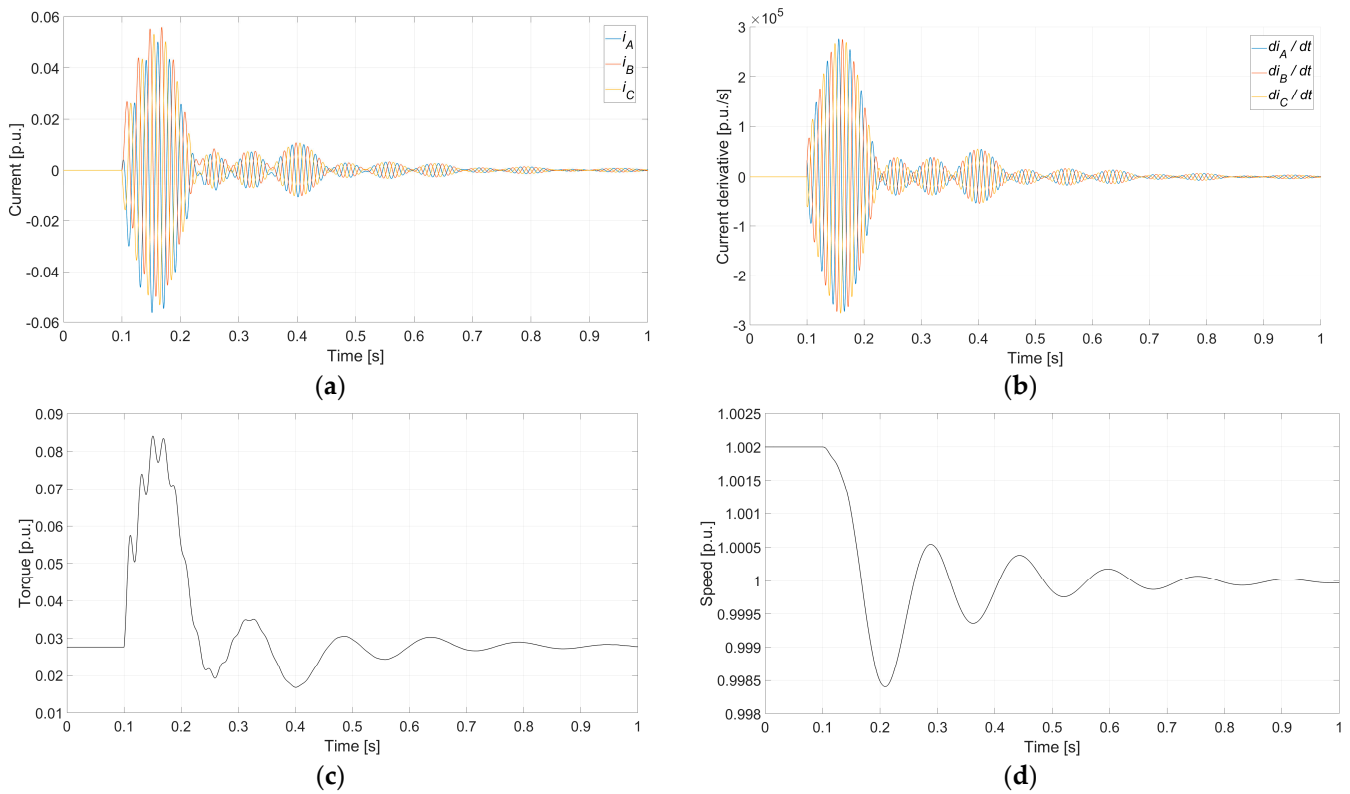
Figure 8. Ideal synchronization (Case 1: $\Delta U_0 = 0\%$, $\Delta \delta_0 = 0°$, and $\Delta f_0 = 0.1$ Hz) conducted at $t = 0.1$ s: (**a**) instantaneous current for each phase; (**b**) instantaneous current derivative for each phase; (**c**) electromagnetic torque; and (**d**) rotor speed.

In contrast, Case 2, representing the worst-case scenario still within regulatory limits, demonstrated significantly larger transient responses. After the CB closing at $t = 0.1$ s, the current peaks reached approximately 80% of the rated current in the first half-cycle, as shown in Figure 9a, which is 13.3 times higher than the current peak observed in Case 1. The current derivative surged to around 2.2×10^6 p.u./s, as seen in Figure 9b, approximately 7.85 times the value observed in Case 1. According to the peak values achieved in this case, the threshold settings of the proposed protection method can be adjusted at $i_{SET} = 0.8$ p.u. and $di/dt_{SET} = 2.2 \times 10^6$ p.u./s for the highest sensitivity.

Similarly, the electromagnetic torque in Case 2 exhibited much higher oscillations, peaking at 83% of the rated value, as derived from Figure 9c, almost 10 times greater than the torque observed in Case 1. Despite these large transient magnitudes, the rotor speed stabilizes at 1 p.u. with the system reaching a steady state around 1 s after synchronization, as per Figure 9d. Thereby, the time parameter of the proposed protection method can be set at $T_{SET} = 1$ s.

These findings show that for synchronizations at the tolerance limits, the current, current derivatives, and torque experience significantly higher peaks compared to ideal conditions in Case 1, as the parameter mismatches are more notable.
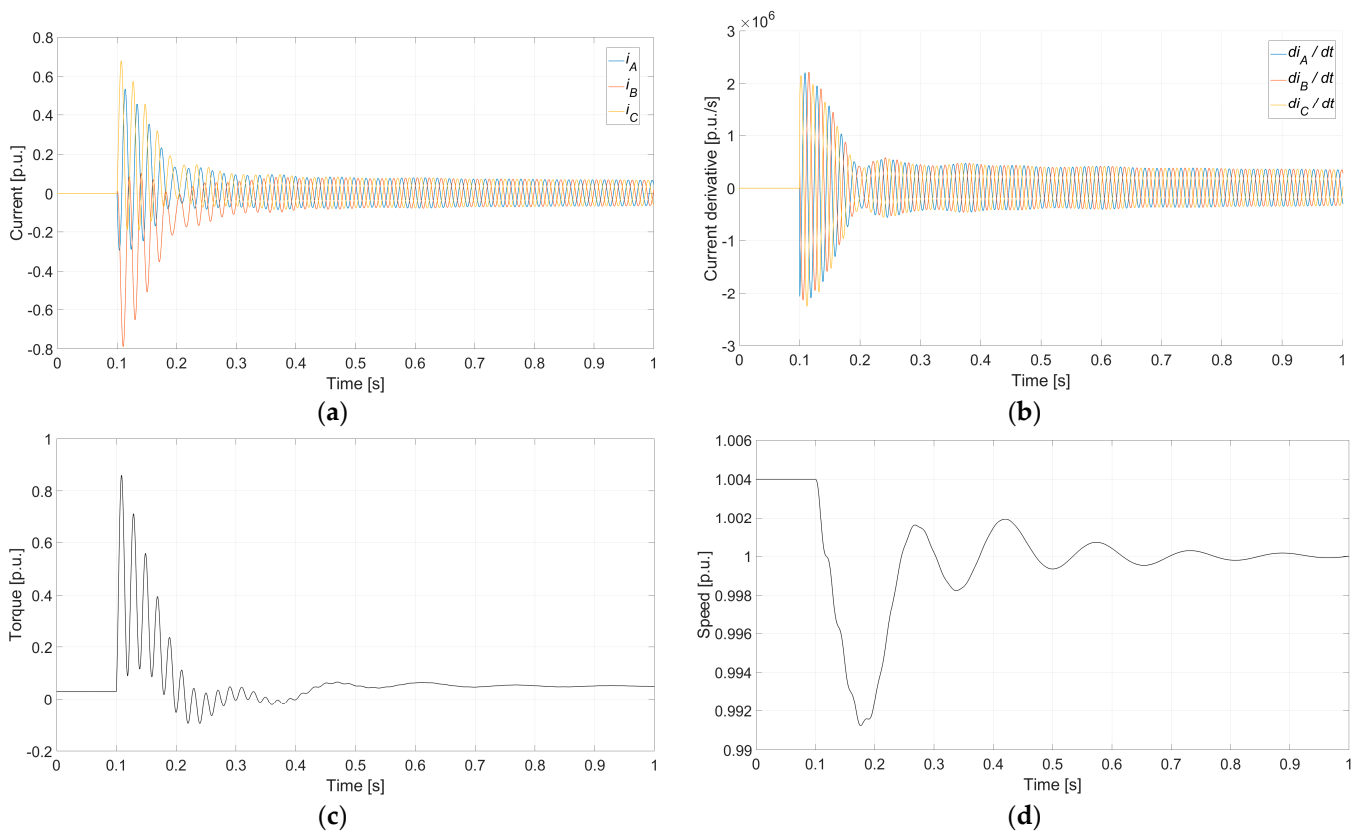
Figure 9. Synchronization at the limits of the tolerance window (Case 2: $\Delta U_0 = 10\%$, $\Delta \delta_0 = 10°$, and $\Delta f_0 = 0.2$ Hz) conducted at $t = 0.1$ s: (**a**) the instantaneous current for each phase; (**b**) the instantaneous current derivative for each phase; (**c**) the electromagnetic torque; and (**d**) the rotor speed.

5.3. Faulty Synchronizations

After having verified that the system responds accurately to correct synchronizations and having set the pickup and time delay values, several faulty synchronization scenarios were simulated to verify the performance of the proposed method. These simulations were conducted with equal voltage magnitudes on both sides of the CB ($\Delta U_0 = 0\%$, a condition easily ensured by any automatic synchronizer), a small frequency difference ($\Delta f_0 = 0.1$ Hz), and varying phase angle mismatches. As outlined in Section 3, out-of-phase situations, usually caused by wiring errors, are not detectable by synchro-check relays, making them the most critical issue to address. The phase angle mismatches for out-of-phase synchronizations correspond to $\Delta \delta_0 = 60°$ (Case 3), $\Delta \delta_0 = 120°$ (Case 4), or $\Delta \delta_0 = 180°$ (Case 5) depending on the type of wiring error. The resulting current waveforms as well as the current-derivative waveforms for each phase are presented for Cases 3, 4, and 5 in Figures 10–12, respectively.

From Figures 10a, 11a and 12a, it can be observed that once the CB is closed at $t = 0.1$ s, the generator currents surge to approximately 3.5, 6, and 7 p.u. for Cases 3, 4, and 5, respectively. As expected, the peak current magnitude increases with larger phase angle mismatches. In the least severe scenario (Case 3), the instantaneous current value of 3.5 p.u. represents roughly 4.37 times the value seen in a proper synchronization at the tolerance window limit (0.8 p.u. for Case 2). In the most severe scenario (Case 5), the generator currents reach approximately 700% of the rated current, which is double the value observed during the correct synchronization at the tolerance window limit (Case 2). These results confirm the effectiveness of the instantaneous current value-based tripping criteria in detecting synchronization faults.
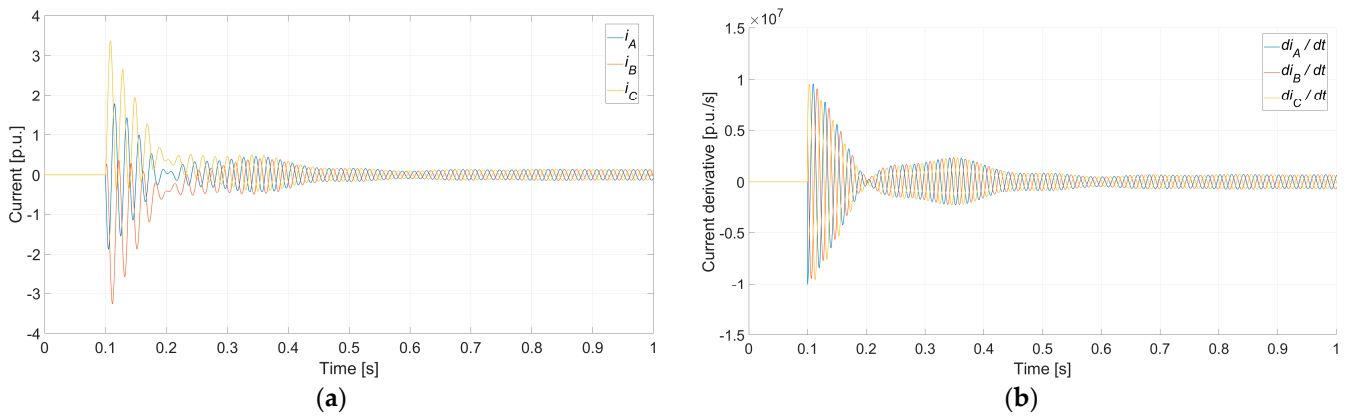
Figure 10. Faulty synchronization (Case 3: $\Delta U_0 = 0\%$, $\Delta \delta_0 = 60°$, and $\Delta f_0 = 0.1$ Hz) conducted at $t = 0.1$ s: (**a**) instantaneous current for each phase; (**b**) instantaneous current derivative for each phase.
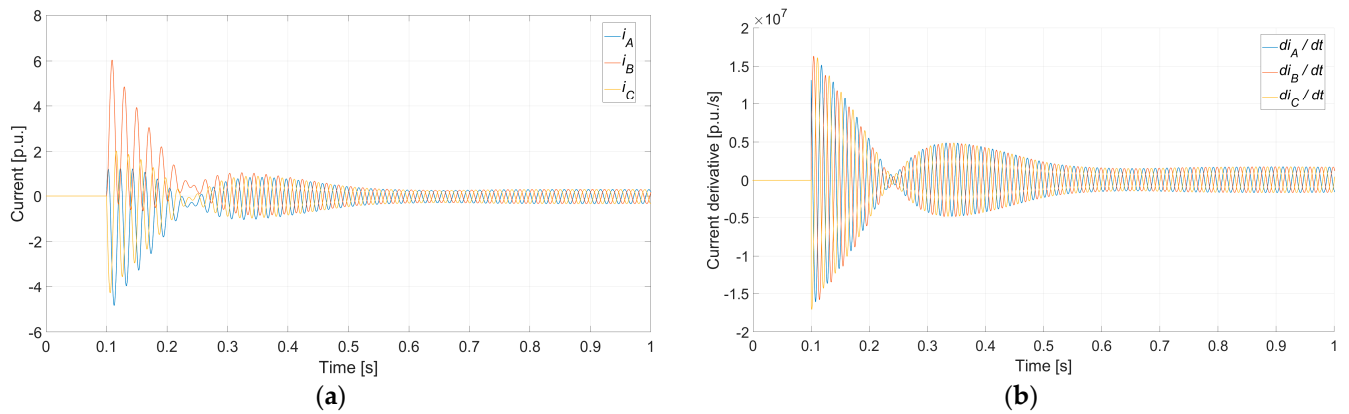
Figure 11. Faulty synchronization (Case 4: $\Delta U_0 = 0\%$, $\Delta \delta_0 = 120°$, and $\Delta f_0 = 0.1$ Hz) conducted at $t = 0.1$ s: (**a**) instantaneous current for each phase; (**b**) instantaneous current derivative for each phase.
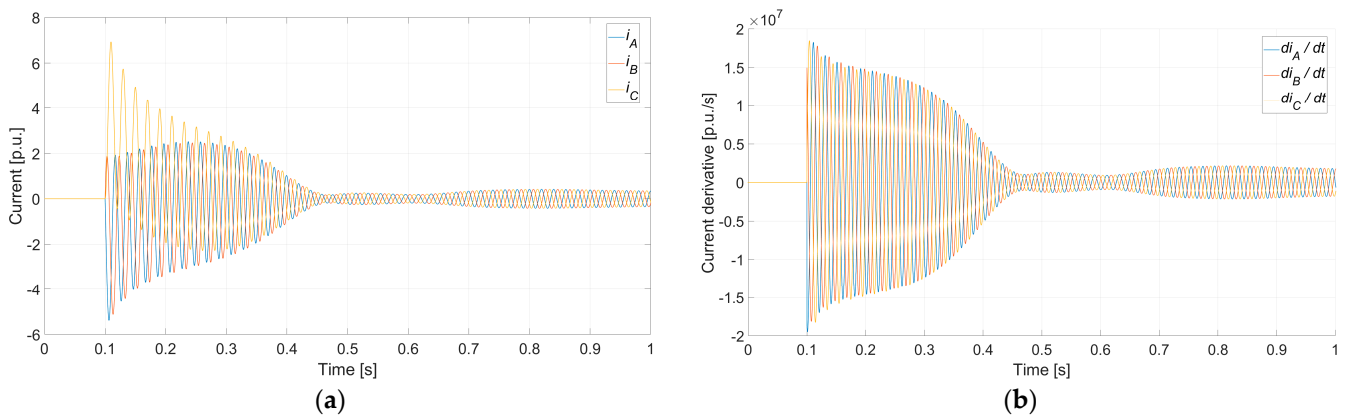
Figure 12. Faulty synchronization (Case 5: $\Delta U_0 = 0\%$, $\Delta \delta_0 = 180°$, and $\Delta f_0 = 0.1$ Hz) conducted at $t = 0.1$ s: (**a**) instantaneous current for each phase; (**b**) instantaneous current derivative for each phase.

Similarly, from Figures 10b, 11b and 12b, it is observed that after the CB closes at $t = 0.1$ s, the current derivatives rise to approximately 1×10^7, 1.7×10^7, and 1.9×10^7 p.u./s for Cases 3, 4, and 5, respectively. As with the currents, the peak derivative values increase with greater phase angle differences. In the least severe scenario (Case 3), the instantaneous derivative value of 1×10^7 p.u./A is approximately 4.5 times the derivative value for a correct synchronization at the tolerance window (2.2×10^6 p.u./s for Case 2). In the

worst-case scenario (Case 5), the current derivatives nearly double, reaching 8.6 times the value observed in Case 2. This clearly demonstrates the applicability of the instantaneous current-derivative value-based tripping criteria for detecting faulty synchronizations.

The operation of the proposed protective schemes for Case 5 is illustrated in detail in Figure 13. The thresholds have been set according to the values of Case 2. The points where the tripping criteria are met are indicated in Figure 13. For the current-based scheme (Figure 13a), it is observed that the last phase (phase C) meets the tripping criteria approximately 2.5 ms after synchronization occurs at $t = 0.1$ s. In contrast, the current-derivative-based scheme activates immediately after synchronization at $t = 0.1$ s due to the sharp surge detected in the current-derivative calculation. Therefore, it is verified that the proposed method based on instantaneous current values performs significantly faster fault detection compared to state-of-the-art RMS-based overcurrent schemes, with detection times that do not exceed 2.5 ms.
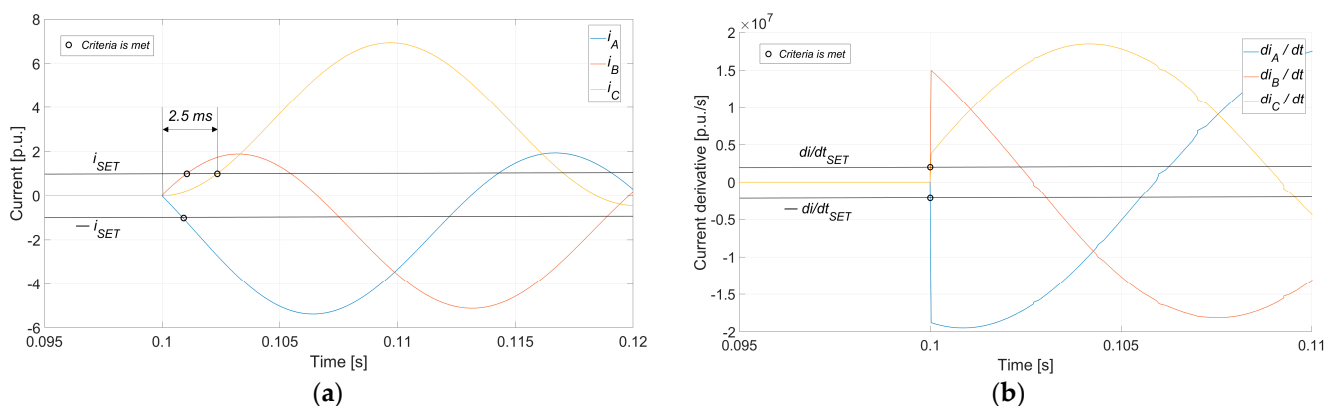
Figure 13. Faulty synchronization (Case 5: $\Delta U_0 = 0\%$, $\Delta \delta_0 = 180°$, and $\Delta f_0 = 0.1$ Hz) conducted at $t = 0.1$ s: (**a**) the detailed operation of the protective scheme based on the instantaneous current value; (**b**) the detailed operation of the protective scheme based on the instantaneous current-derivative value.

Additionally, a deliberate delay of $\varepsilon = 1$ ms can be introduced to prevent false tripping, ensuring more reliable protection. In all cases, once the tripping criteria are satisfied, it is verified that the conditions (instantaneous current or current-derivative values exceeding their respective thresholds) remain fulfilled throughout this time delay.

Once the tripping criteria are met, the protective schemes trigger the opening of the CB to clear the fault. Assuming a CB opening time of 50 ms, the circuit is opened no later than 53.5 ms after synchronization (2.5 ms for fault detection in phase C—the last phase in which the tripping criteria is met according to the instantaneous current value-based scheme, i.e., the longest fault detection time or worst-case scenario—1 ms for the intentional delay, and 50 ms for the CB to open). As shown in Figure 14a, the flow of high fault currents is thus limited to 53.5 ms after synchronization, effectively reducing the duration of electrical stress. Additionally, as seen in Figure 14b, the torque oscillations are significantly shortened, minimizing the risk of mechanical damage to the system. It is concluded that the proposed protection method reduces the fault detection time to only a few ms, which is an order of magnitude lower than conventional CB opening times. Having achieved fault detection time optimization, the performance of switchgear technology is left as the primary limiting factor for rapid fault clearance.
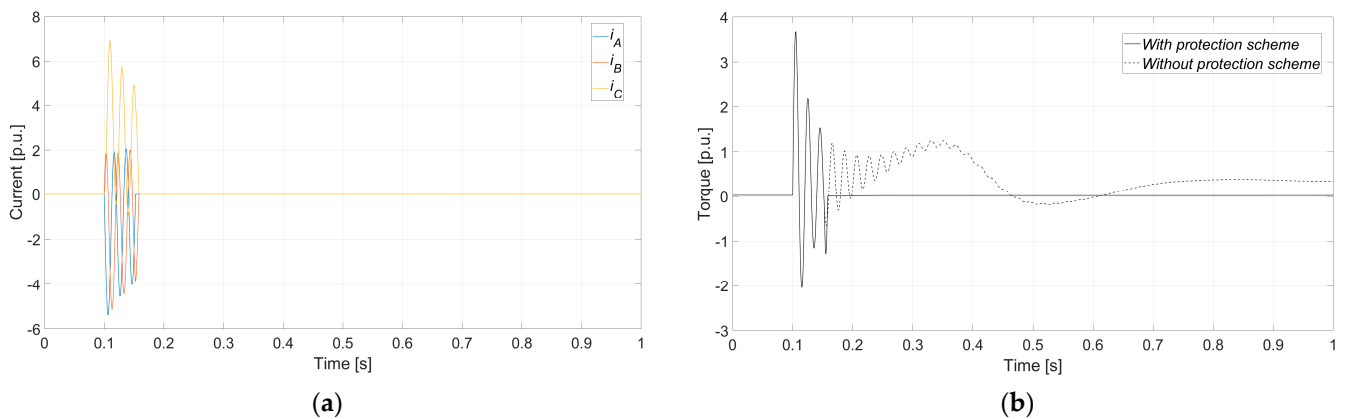
Figure 14. Faulty synchronization (Case 5: $\Delta U_0 = 0\%$, $\Delta \delta_0 = 180°$, and $\Delta f_0 = 0.1$ Hz) conducted at $t = 0.1$ s: (**a**) current waveforms, including tripping; (**b**) torque with and without protective tripping. The CB closing time is considered to be 50 ms.

6. Experimental Tests

6.1. Experimental Test Bench

In order to validate the effectiveness of the proposed protection schemes, a series of tests were conducted on an experimental test bench equipped with a 5 kVA synchronous generator unit. A simplified single-line diagram of the experimental setup is presented in Figure 15a, while an overview of the setup highlighting its key components is shown in Figure 15b.
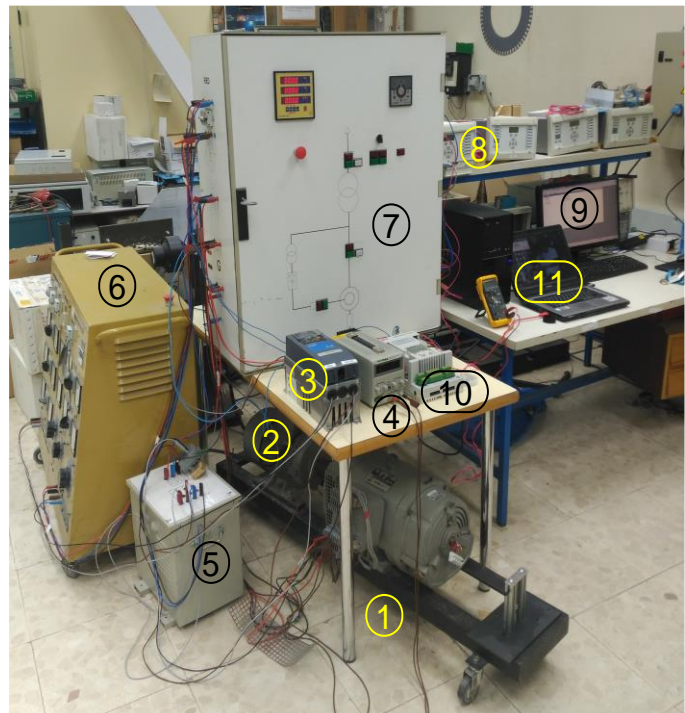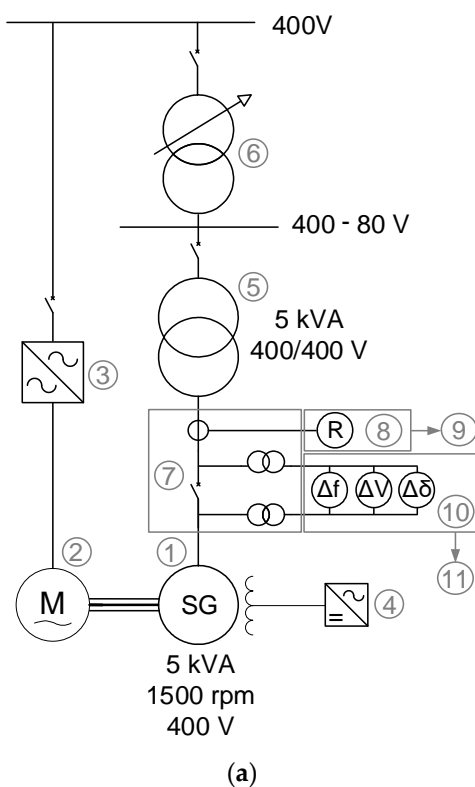
Figure 15. Experimental setup: (**a**) single-line diagram; (**b**) overview.

The experimental tests were conducted on a 5 kVA four-pole SG (1), driven by an induction motor (2) powered by a variable frequency drive (VFD) (3). The excitation power was supplied by an independent DC power source (4). The SG was connected to the grid

via a 5 kVA 1:1 power transformer (5) at an adjustable voltage up to 400 V. This voltage range for the connection bus was achieved through an adjustable three-phase power supply based on an autotransformer (6), allowing faulty synchronization tests to be performed at reduced system voltage, thereby preventing potential damage to the machine.

The generator CB and current transformers (CTs) as well as the voltage transformers (VTs) on both sides of the CB were housed within a custom-designed switchgear cabinet (7), specifically developed for conducting synchronization tests in the laboratory environment. The secondary side of the CT was connected to a MiCOM P343® (Areva T&D, Paris, France) digital multifunction relay (8), covering the main SG protective relaying functions and also serving as a fault recorder, with data captured via a computer (9). The synchronization tests under different conditions were carried out using the digital synchronizer function of an Unitrol 1020 ® (ABB, Zurich, Switzerland) automatic voltage regulator (10), also interfaced through a computer (11).

6.2. Experimental Results

6.2.1. Correct Synchronization Tests at Rated Voltage (100%/400 V)

First, in order to verify the correct synchronization conditions, several experimental tests were conducted under various conditions, all within the specified tolerance window for each parameter. As expected, when the synchronization parameters closely align with the ideal values—such as zero phase angle difference ($\Delta\delta_0 \approx 0°$), zero voltage difference ($\Delta U_0 \approx 0\%$), and zero frequency difference ($\Delta f_0 \approx 0$ Hz)—the synchronization currents remain negligible. However, as the parameters deviate from these ideal points at the moment of CB closing, the current magnitudes increase accordingly. For instance, the phase angle and voltage difference limits set by the SG manufacturer ($\Delta\delta_0 = 15°$ and $\Delta U_0 = 5\%$) are used as a reference baseline for the threshold settings in the experimental developments. In these non-ideal but acceptable synchronization conditions, a small frequency difference is necessarily considered ($\Delta f_0 = 0.1$ Hz).

Figure 16 presents the behavior of the instantaneous synchronization currents for each phase (Figure 16a) as well as the evolution of their instantaneous time derivatives (Figure 16b). In this scenario, the currents surge to nearly their rated value after CB closing. Following the transient phase, the currents stabilize at approximately 0.1 p.u. in the steady state, which corresponds to the active power supplied by the induction motor, operating at 50.10 Hz and 1500 rpm. The instantaneous current derivatives also show a significant response, with a peak value in the first half-cycle of 295 p.u./s.

(a) (b)
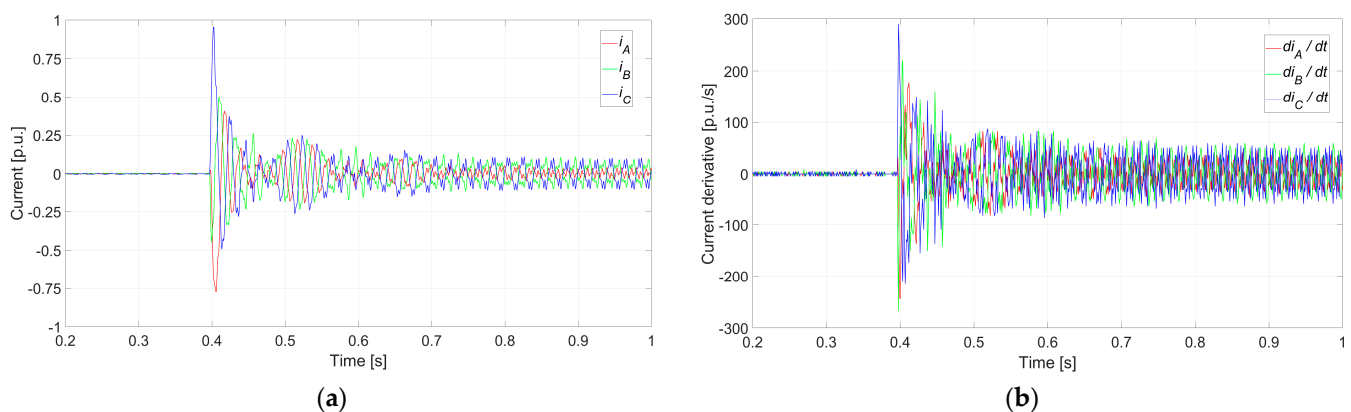
Figure 16. Correct synchronization ($\Delta U_0 = 5\%$, $\Delta\delta_0 = 15°$, and $\Delta f_0 = 0.1$ Hz): (**a**) current waveforms; (**b**) current-derivative waveforms.

According to the healthy condition experimental tests, the threshold settings of the proposed protection method can be adjusted to $i_{SET} = 1$ p.u. and $di/dt_{SET} = 295$ p.u./s for the highest sensitivity. The protection activation time period can be set to $T_{SET} = 0.3$ s.

Overall, the results demonstrate that under marginal synchronization conditions, both current and current derivatives exhibit sharp increases following CB closing. However, the short-circuit capacity of the grid and the impedance of the primary power transformer significantly influence the value of these currents and their time evolution. Therefore, a case-by-case analysis, as conducted in this experimental approach, is required to set threshold parameters accurately based on a healthy baseline synchronization. In the industry, this baseline synchronization shall be performed during protection commissioning in real operational conditions.

6.2.2. Faulty Synchronization Tests at Reduced Voltage (20%/80 V)

In the faulty synchronization tests, the bus voltage was intentionally reduced using the adjustable power supply to prevent potential damage to the SG under test. The voltage level was carefully chosen to ensure that the SG's rated current was not significantly exceeded. After several iterations, a voltage reduction to 20% of the nominal value (80 V) was selected as optimal. As the voltage is reduced, the resulting currents decrease in nearly the same proportion, satisfying a direct relationship between voltage reduction and current attenuation. In fact, the tripping thresholds can be set on the p.u. system based on the correct synchronization tests at rated voltage (100%/400 V) and then applied correspondingly to the faulty synchronization tests at reduced voltage (20%/80 V).

The faulty synchronization tests were carried out to emulate out-of-phase situations due to incorrect wirings in the automatic synchronizer. The tests were conducted both with and without the proposed protection schemes in place. In the following, two specific scenarios, involving initial phase angle differences of $\Delta\delta_0 = 120°$ and $\Delta\delta_0 = 180°$, have been selected for detailed analysis. All other synchronization conditions, such as voltage difference and frequency difference, were maintained within acceptable limits of $\Delta U_0 = 2\%$ and $\Delta f_0 = 0.1$ Hz, respectively. Figures 17 and 18 show the synchronization currents through each phase for the cases of $\Delta\delta_0 = 120°$ and $\Delta\delta_0 = 180°$, respectively.

(a)   (b)
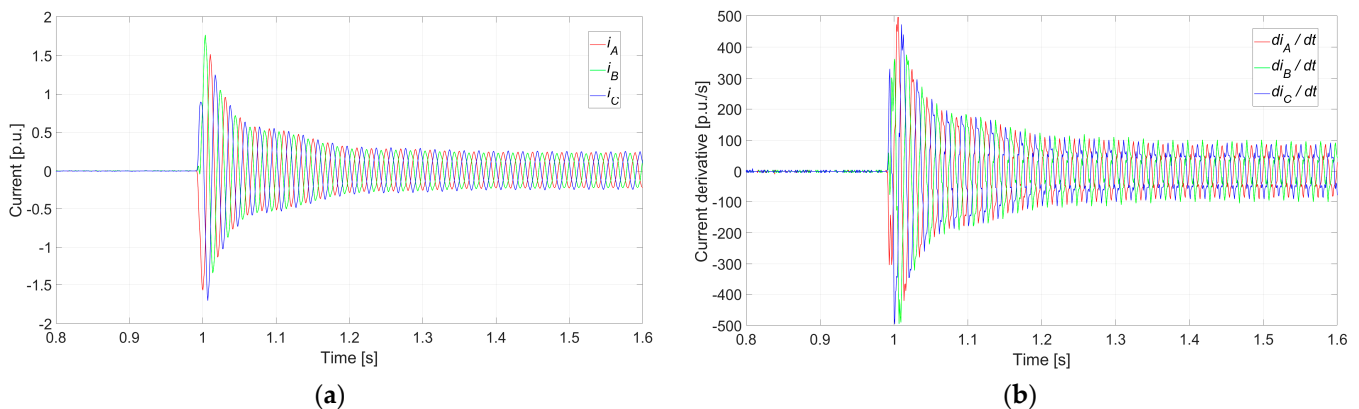
Figure 17. Faulty synchronization ($\Delta U_0 = 2\%$, $\Delta\delta_0 = 120°$, and $\Delta f_0 = 0.1$ Hz): (**a**) current waveforms; (**b**) current-derivative waveforms.

As observed in Figures 17a and 18a, the currents peak at 1.76 and 2.35 p.u. for faulty synchronizations with $\Delta\delta_0 = 120°$ and $\Delta\delta_0 = 180°$, respectively. These values significantly exceed the rated current even at just 20% of the rated voltage. Based on the principle of proportionality, it is anticipated that at full-rated voltage, the currents' peaks could reach 8.8 and 11.75 times the value for correct synchronization, as discussed in the previous section, which is adopted as a reference. Following the transient phase, the currents stabilize at approximately 0.20 p.u. in the steady state, corresponding to the active power contribution of the induction motor, which continues operating at 50.10 Hz and 1500 rpm. As expected, greater phase mismatches result in higher synchronization currents after CB closing, thus increasing the risk of damage to power generation equipment and affecting

grid stability. This includes the potential tripping of other parallel SGs, power oscillations, and voltage sags.
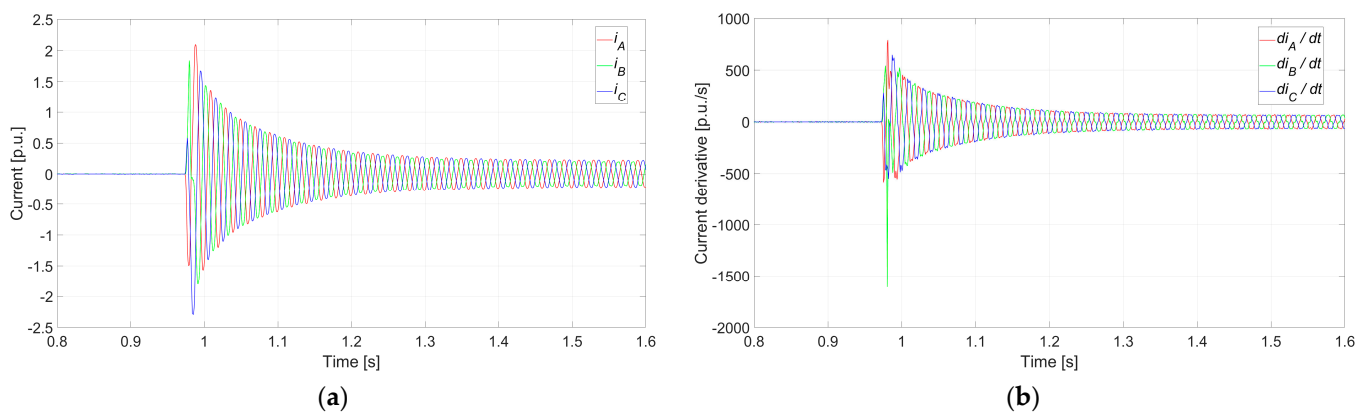
Figure 18. Faulty synchronization ($\Delta U_0 = 2\%$, $\Delta \delta_0 = 180°$, and $\Delta f_0 = 0.1$ Hz): (**a**) current waveforms; (**b**) current-derivative waveforms.

Additionally, as shown in Figures 17b and 18b, the current derivatives reach peak absolute values of approximately 500 and 1630 p.u./s for synchronizations with $\Delta \delta_0 = 120°$ and $\Delta \delta_0 = 180°$, respectively. Similar to the currents, the peak derivative values also increase with larger phase angle mismatches. Even at 20% of the rated voltage, the current-derivative peaks are 1.6 and 5.4 times higher than the peak derivative values for correct synchronization, which serves as the reference for threshold setting. After the transient phase, the current derivative stabilizes below 100 p.u./s in all cases.

However, the derivative peak observed at 1630 p.u./s in phase B is considered a glitch in the derivative calculation. Instead, a value around 800 p.u./s, consistent with the three-phase system, is anticipated for the corresponding actual derivative peak. This observation underscores the significance of derivative calculations in noisy environments or in systems operating at very high sampling rates. The excessive reduction of the time step ($\Delta t \to 0$) used in the derivative computation as per Equation (14) results in increased sensitivity to measurement noise. Conversely, significantly increasing the time step enhances the stability and reliability of the derivative calculation but slows the method's response. A viable trade-off solution is to use the average derivative values from multiple instantaneous current measurements uniformly distributed within the original sampling period *T*, as expressed in Equation (16).

The operation of the proposed protective schemes for the case of $\Delta \delta_0 = 180°$ is detailed in Figure 19. The thresholds are set based on the peak current and current-derivative values for the correct synchronization, as discussed in the previous section. The points where the tripping criteria are met are indicated in Figure 19. For the current-based scheme (Figure 19a), the first phase to meet the tripping criteria (phase A) does so approximately 2.5 ms after synchronization, while the last phase (phase C) reaches the threshold approximately 7.5 ms after synchronization. In contrast, the current-derivative-based scheme (Figure 19b) is triggered earlier, with phase A meeting the tripping condition just 2 ms after synchronization due to the immediate sharp increase in the current derivative. For the last phase to meet the tripping condition (phase C), the detection is produced approximately 6 ms after synchronization.

Therefore, it is experimentally verified that the proposed method based on instantaneous current values performs significantly faster fault detection compared to state-of-the-art RMS-based overcurrent schemes, ensuring detection times as short as 2–2.5 ms.

As aforementioned, to enhance protection reliability, a deliberate delay of $\varepsilon = 1$ ms can be introduced to prevent false tripping. This ensures more accurate protection performance. In all cases, once the tripping criteria are met, it is confirmed that the conditions

(instantaneous current or current-derivative values exceeding their respective thresholds) remain satisfied throughout the time delay period.

(a)

(b)
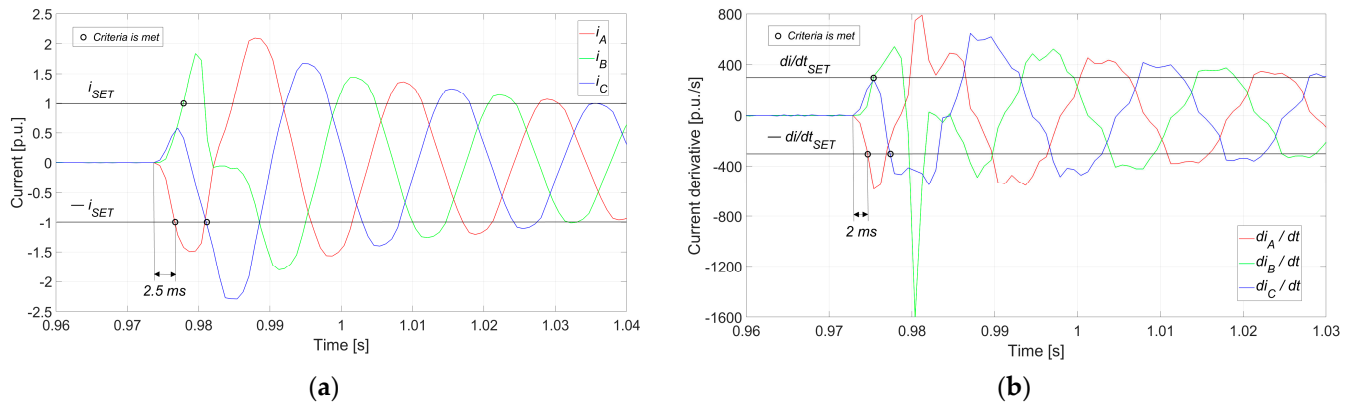
Figure 19. Faulty synchronization ($\Delta U_0 = 2\%$, $\Delta \delta_0 = 180°$, and $\Delta f_0 = 0.1$ Hz): (**a**) the detailed operation of the protective scheme based on instantaneous current value; (**b**) the detailed operation of the protective scheme based on instantaneous current-derivative value.

Once the tripping criteria are met, the protective schemes initiate the opening of the CB to clear the fault. In the experimental test bench, the CB was independently tested, with an opening time measured at 55 ms. Taking into account the longest time delay, the circuit is opened no later than 63.5 ms after synchronization (7.5 ms for fault detection in phase C—the last phase in which the tripping criteria is met according to the instantaneous current value-based scheme, i.e., the longest fault detection time or worst-case scenario, and 55 ms for the CB to open). This operation case is shown in Figure 20 for the cases of $\Delta \delta_0 = 120°$ (Figure 20a) and $\Delta \delta_0 = 180°$ (Figure 20b).

(a)

(b)
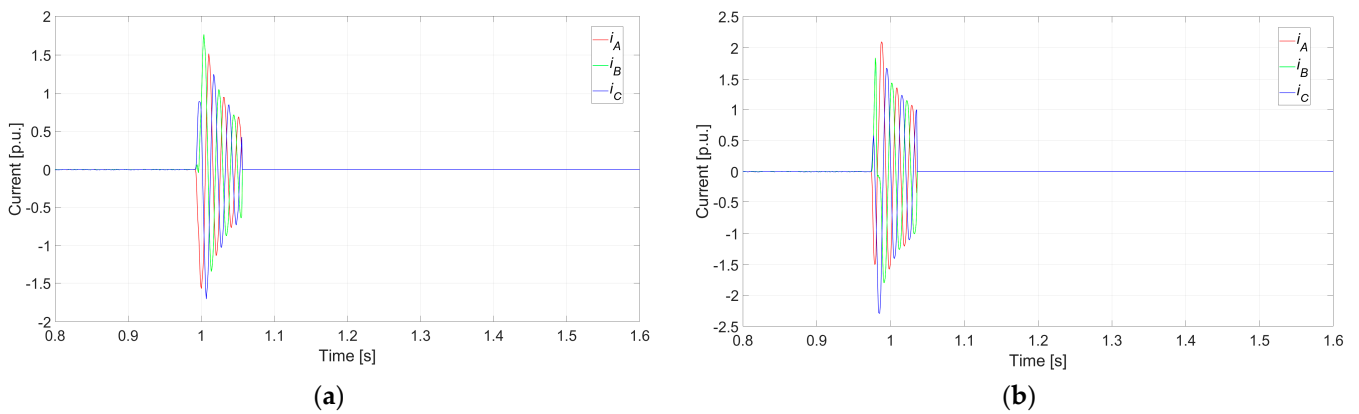
Figure 20. Current waveforms for faulty synchronizations, including tripping: (**a**) $\Delta U_0 = 2\%$, $\Delta \delta_0 = 120°$, and $\Delta f_0 = 0.1$ Hz; (**b**) $\Delta U_0 = 2\%$, $\Delta \delta_0 = 180°$, and $\Delta f_0 = 0.1$ Hz. The CB closing time is 55 ms.

The high fault currents are limited to 63.5 ms after synchronization, effectively reducing the duration of electrical stress. This prompt action significantly shortens torque oscillations, minimizing the risk of mechanical damage to the system. The protective schemes are shown to quickly detect and clear the fault, cutting off both electrical and mechanical stress in a timely manner. However, the initial impact of a faulty synchronization cannot be fully avoided by any protective system, even with fast detection times of 2–2.5 ms as the ones achieved with the proposed schemes, as the primary limiting factor in practice is the CB opening time.

In conclusion, the experimental results demonstrate the effectiveness of the proposed protective schemes in rapidly detecting and clearing synchronization faults. With detection times as short as 2–2.5 ms, the duration of high fault currents and associated electrical stress is significantly reduced. This prompt response also mitigates torque oscillations, minimizing the risk of mechanical damage. However, while the schemes provide fast and reliable protection, the CB opening time remains the limiting factor in fully preventing the initial impact of faulty synchronizations.

7. Conclusions

Faulty synchronizations of SGs can lead to significant electrical and mechanical damage if not mitigated promptly. Existing protection techniques do not allow for faulty synchronization detection in a timely manner so as to trip quickly and avoid these damages. This paper describes the protection needs and provides an analytical framework involving the instantaneous current and current derivative following a faulty synchronization. Based on these markers, two protection schemes are proposed to provide rapid fault detection.

Results from computer simulations and experimental tests demonstrate the effectiveness of the proposed methods. Simulations conducted on a 362 MVA turbo-generator, along with experimental results from a 5 kVA SG, validate the proposed schemes, confirming their capability to provide fast detection of faulty synchronizations following CB closing. This rapid detection significantly reduces the duration of high current stresses and mitigates damaging torque oscillations.

The consistency between computer simulations and experimental tests provides evidence that the proposed methods outperform existing techniques based on RMS overcurrent, enabling faster detection times by circumventing the cycles associated with RMS calculation. The fault detection times achieved in this work are reduced to only 2–2.5 ms after CB closing, leaving the performance of switchgear, mainly the CB, as the only limiting factor for rapid fault clearance. The achievement of faster fault detection is the main practical contribution of this work.

In addition to the contribution in terms of fault detection speed, the use of the current-derivative value for protection against faulty synchronizations represents another novel contribution of this study. The instantaneous current-derivative value-based scheme demonstrated improved performance, detecting faults faster than the instantaneous current value-based scheme due to its heightened sensitivity to swift changes in current after a faulty synchronization.

Both proposed schemes effectively reduce the risk of severe mechanical damage and contribute to overall system stability by minimizing exposure to high fault currents. These advancements represent a significant improvement in the protection of SGs, enhancing the reliability and safety of power systems by addressing a poorly protected fault scenario.

The primary limitations of the proposed method are related to the reliance on instantaneous value-based relaying, which is less established compared to conventional RMS-based relaying technologies. Moreover, despite improving the fault detection time, fault clearance limitations due to the CB still remain.

Future work should explore the integration of these instantaneous protection schemes in the industry, ensuring coordination with existing grid protections. Additionally, testing in larger-scale environments and diverse power system configurations would further assess the scalability and adaptability of the proposed solutions.

Author Contributions: Conceptualization, K.M. and C.A.P.; methodology, K.M. and J.M.G.; software, K.M. and C.A.P.; validation, K.M. and C.A.P.; formal analysis, K.M. and C.A.P.; investigation, K.M. and J.M.G.; resources, C.A.P.; data curation, K.M.; writing—original draft preparation, K.M.; writing— review and editing, K.M., J.M.G., and C.A.P.; visualization, K.M. and J.M.G.; supervision, C.A.P.; project administration, K.M.; funding acquisition, C.A.P. All authors have read and agreed to the published version of the manuscript.

Data Availability Statement: The original contributions presented in this study are included in the article. Further inquiries can be directed to the corresponding author.

Conflicts of Interest: The authors declare no conflicts of interest.

References

1. Eruneo, J.; Chowdhury, R. *Practices for Generator Synchronizing Systems*; Technical Report; IEEE: Piscataway, NJ, USA, 2024; pp. 1–97.
2. Schaefer, R.C. Art of Generator Synchronizing. *IEEE Trans. Ind. Appl.* **2017**, *53*, 751–757. [CrossRef]
3. Hammons, T.J. Stressing of Large Turbine-Generators at Shaft Couplings and LP Turbine Final-Stage Blade Roots Following Clearance of Grid System Faults and Faulty Synchronisation. *IEEE Trans. Power Appar. Syst.* **1980**, *PAS-99*, 1652–1662. [CrossRef]
4. Chen, H.H.; Jablonka, G.E.; Mitsche, J.V.; Lewis, J.B. Turbine-Generator Loss-of-Life Analysis Following a Faulty Synchronization Incident. In Proceedings of the 42nd American Power Conference, Chicago, IL, USA, 21 April 1980.
5. Mitsche, J.V.; Rusche, P.A. Shaft Torsional Stress Due to Asynchronous Faulty Synchronization. *IEEE Trans. Power Appar. Syst.* **1980**, *PAS-99*, 1864–1870. [CrossRef]
6. Gozdowiak, A. Faulty Synchronization of Salient Pole Synchronous Hydro Generator. *Energies* **2020**, *13*, 5491. [CrossRef]
7. Li, W.; Wang, P.; Li, J.; Wang, L.; Gong, S.; Li, D. Influence of Stator Parameter Variation and Phase-Shift Under Synchronizing Out of Phase on Turbine Generator Electromagnetic Field. *IEEE Trans. Energy Convers.* **2017**, *32*, 525–533. [CrossRef]
8. Liu, W.; Li, W.; Wang, P.; Li, D.; Li, Z.; Xu, G. Transient Process Analysis of Multi-Physical Parameters of Turbine Generator During Out of Phase Synchronization Fault. *IEEE Trans. Energy Convers.* **2022**, *37*, 2058–2068. [CrossRef]
9. Manson, S.M.; Upreti, A.; Thompson, M.J. Case Study: Smart Automatic Synchronization in Islanded Power Systems. *IEEE Trans. Ind. Appl.* **2016**, *52*, 1241–1249.
10. Tian, P.; Guerrero, J.M.; Mahtani, K.; Platero, C.A. Instantaneous Specific Protection Method Against Faulty Synchronizations of Synchronous Machines. *IEEE Access* **2021**, *9*, 88868–88878. [CrossRef]
11. Working Group A1.35, Study Committee A1-Power generation and electromechanical energy conversion. Hydrogenators Behaviour Under Transient Conditions. *ELECTRA* **2016**, *288*, 1–4.
12. Nagpal, M.; Gu, L.; Barone, R.; Chowdhury, R.; Thompson, M. A Tale of Two Out-of-Phase Synchronizing Events at BC Hydro. In Proceedings of the 2023 76th Annual Conference for Protective Relay Engineers (CFPR), College Station, TX, USA, 27–30 March 2023.
13. Ransom, D.L. Get in Step With Synchronization. *IEEE Trans. Ind. Appl.* **2014**, *50*, 4210–4215. [CrossRef]
14. Thompson, M.J. Fundamentals and Advancements in Generator Synchronizing Systems. In Proceedings of the 2012 65th Annual Conference for Protective Relay Engineers, College Station, TX, USA, 2–5 April 2012; pp. 203–214.
15. Evans, R.A. A Manual/Automatic Synchronization Circuit for a 37.5 MVA Steam-Turbine-Driven Generator. *IEEE Trans. Ind. Appl.* **1990**, *26*, 1081–1085. [CrossRef]
16. Krause, P.C.; Hollopeter, W.C.; Triezenberg, D.M.; Rusche, P.A. Shaft Torques During Out-of-Phase Synchronization. *IEEE Trans. Power Appar. Syst.* **1977**, *96*, 1318–1323. [CrossRef]
17. Strang, W.M.; Mozina, C.J.; Beckwith, B.; Beckwith, T.R.; Chhak, S.; Fennell, E.C.; Kalkstein, E.W.; Kozminski, K.C.; Pierce, A.C.; Powell, P.W.; et al. Generator Synchronizing Industry Survey Results. *IEEE Trans. Power Deliv.* **1996**, *11*, 174–183. [CrossRef]
18. Canay, I.M.; Braun, D.; Koeppl, G.S. Delayed Current Zeros Due to Out-of-Phase Synchronizing. *IEEE Trans. Energy Convers.* **1998**, *13*, 124–132. [CrossRef]
19. Canay, I.M.; Rohrer, H.J.; Schnirel, K.E. Effect of Electrical Disturbances, Grid Recovery Voltage and Generator Inertia on Maximization of Mechanical Torques in Large Turbogenerator Sets. *IEEE Trans. Power Appar. Syst.* **1980**, *99*, 1357–1370.
20. Barner, K.; Klingerman, N.; Thompson, M.; Chowdhury, R.; Finney, D.; Samineni, S. OOPS, Out-of-Phase Synchronization. In Proceedings of the 46th Annual Western Protective Relay Conference, Spokane, WA, USA, 22–24 October 2019.
21. *IEEE Std C50.12 (Previously Designated as ANSI C50.12-1982)*; IEEE Standard for Salient-Pole 50 Hz and 60 Hz Synchronous Generators and Generator/Motors for Hydraulic Turbine Applications Rated 5 MVA and Above. IEEE: Piscataway, NJ, USA, 2006; pp. 1–45.
22. *IEEE Std C50.13-2014 (Revision of IEEE Std C50.13-2005)*; IEEE Standard for Cylindrical-Rotor 50 Hz and 60 Hz Synchronous Generators Rated 10 MVA and Above. IEEE: Piscataway, NJ, USA, 2014; pp. 1–63.
23. Reimert, D. *Protective Relaying for Power Generation Systems*, 1st ed.; CRC Press: Boca Raton, FL, USA, 2017.
24. *IEEE Std C57.12.00-2015 (Revision of IEEE Std C57.12.00-2010)*; IEEE Standard for General Requirements for Liquid-Immersed Distribution, Power, and Regulating Transformers. IEEE: Piscataway, NJ, USA, 2016; pp. 1–74.
25. *IEEE Std C37.102-2023 (Revision of IEEE Std C37.102-2006)*; IEEE Guide for AC Generator Protection. IEEE: Piscataway, NJ, USA, 2024; pp. 1–211.
26. Raghul, S.J.; Vanaja, I.; Rajini, V.; TamilSelvi, S.; Babu, K.N.D. Synergistic Integration of Power System Protection and Electrical Machine Operation Paradigms: A Comprehensive Framework Study. In Proceedings of the 2024 IEEE 5th India Council International Subsections Conference (INDISCON), Chandigarh, India, 22–24 August 2024; pp. 1–6.

27. Stelmashchuk, S.V. Using the Coordinated Control Method in the Problem of Synchronization of Synchronous Generators of Power Plants. In Proceedings of the 2020 International Multi-Conference on Industrial Engineering and Modern Technologies (FarEastCon), Vladivostok, Russia, 6–7 October 2020; pp. 1–6.

28. Al-Soud, M.; Awwad, A.; Al-Quteimat, A.; Ushkarenko, O. Fuzzy Logic-Based Synchronization Control System of Generators under Conditions of Frequency Instability. *Bull. Electr. Eng. Inform.* **2023**, *12*, 3215–3227. [CrossRef]

29. Shi, K.; Song, W.; Ge, H.; Xu, P.; Yang, Y.; Blaabjerg, F. Transient Analysis of Microgrids with Parallel Synchronous Generators and Virtual Synchronous Generators. *IEEE Trans. Energy Convers.* **2020**, *35*, 95–105. [CrossRef]

30. Ajala, O.; Domínguez-García, A.D.; Liberzon, D. Robust Leader–Follower Synchronization of Electric Power Generators. *Syst. Control Lett.* **2021**, *152*, 104937. [CrossRef]

31. Siddiquee, A.; Islam, T.; Shahriar, S.; Sikder, B.; Ghosh, A.; Reza, M.S. Automatic Synchronization of a Newly Installed Generator to Infinite Bus of Bangladesh Power System. In Proceedings of the 2019 International Conference on Sustainable Technologies for Industry 4.0 (STI), Dhaka, Bangladesh, 24–25 December 2019; pp. 1–4.

32. Mikhailov, D.P.; Kim, A.A.; Grinishena, S.A.; Lukichev, A.N. Automatic Synchronization System for Synchronous Generators. In Proceedings of the 2022 Conference of Russian Young Researchers in Electrical and Electronic Engineering (ElConRus), Saint Petersburg, Russian Federation, 25 January 2022; pp. 782–785.

33. Saranathan, M.; Ravi, A.; Dinesh Babu, K.N.; Rajini, V.; Krishna Achuthan Parthasarathy, H.; Tamilselvi, S. Automatic Synchronization of Alternator Using Numerical Relays. In Proceedings of the 2022 IEEE 2nd Mysore Sub Section International Conference (MysuruCon), Mysuru, India, 16–17 October 2022; pp. 1–7.

34. Siddiqi, M.T.A.; Rasul, M.M.; Hossain, S.M. Automatic Synchronization Unit for Marine Alternators. In Proceedings of the 2021 2nd International Conference on Robotics, Electrical and Signal Processing Techniques (ICREST), Dhaka, Bangladesh, 5–7 January 2021; pp. 211–214.

35. Kirichenko, V.F.; Fyodorova, V.A.; Rusina, A.G.; Glazyrin, G.V. Improving Methods for Synchronizing Generators. In Proceedings of the 2023 IEEE 24th International Conference of Young Professionals in Electron Devices and Materials (EDM), Novosibirsk, Russian Federation, 29 June–3 July 2023; pp. 1060–1063.

36. Mahmoud, R.A.A. Smart Automatic Synchronization System Based on Coherence Algorithm for Power Grids. *J. Eng.* **2023**, *2023*, e12214. [CrossRef]

37. Allah, R.A. Correlation-Based Synchro-Check Relay for Power Systems. *IET Gener. Transm. Distrib.* **2018**, *12*, 1109–1120. [CrossRef]

38. *IEEE Std 421.5-2016*; IEEE Recommended Practice for Excitation System Models for Power System Stability Studies. IEEE: Piscataway, NJ, USA, 2016; pp. 1–207. Available online: https://ieeexplore.ieee.org/document/755342 (accessed on 25 November 2024).

39. Gobierno de España. *Orden de 5 de Septiembre de 1985 por la que se Establecen Normas Administrativas y Técnicas para Funcionamiento y Conexión a las Redes Eléctricas de Centrales Hidroeléctricas de Hasta 5.000 KVA y Centrales de Autogeneración Eléctrica. Spanish Regulation*; Gobierno de España: Madrid, Spain, 1985.